Characteristic Model Based All-Coefficient Adaptive Control on Flexible Rotor Supported by Active Magnetic Bearings

---

A Thesis

Presented to

the faculty of the School of Engineering and Applied Science

University of Virginia

---

in partial fulfillment

of the requirements for the degree

Master of Science

by

Long Di

May

2013

APPROVAL SHEET

The thesis

is submitted in partial fulfillment of the requirements

for the degree of

Master of Science

Long Di

AUTHOR

The thesis has been read and approved by the examining committee:

Zongli Lin

Advisor

Gang Tao

Timothy Dimond

Accepted for the School of Engineering and Applied Science:

James H. Ay

Dean, School of Engineering and Applied Science

May

2013

Abstract

Active magnetic bearings (AMBs) have found a wide range of high-speed rotating machinery applications in energy storage, electric power generation, machine tool operation, heart pumps and hybrid vehicles. Compared with conventional mechanical bearings, AMBs need feedback control to support and constrain the rotor and demand additional electronic devices.

When AMBs are used to support flexible rotors, their nonlinear characteristics and complex dynamics of flexible rotors cause problems with stabilization and disturbance rejection. Proportional-integral-derivative (PID) controllers are the most popular control method for AMB applications. They are easy to implement and reasonable control performance can be achieved. However, it is difficult for PID controllers to deliver robust and near optimal performance for complex dynamic systems. In recent years, robust control techniques such as μ-synthesis have also been applied to AMB applications. The μ-synthesis is able to better handle the uncertainties in complex systems and to achieve reliable performance. However, it requires plant and uncertainty models to generate the most suitable solution, which makes this control design not as practical as PID controllers.

The characteristic model-based all-coefficient adaptive control (ACAC) method has been widely used in process control and the aerospace industry. Numerous applications have demonstrated its effectiveness. This method is able to provide robust control performance on multidimensional complex dynamical systems, while maintaining a simple structure and not requiring the actual plant model. It focuses on the characteristics of the plant and the control performance requirements instead of precise system dynamics. It compresses the corresponding information of the high order plant into several characteristic parameters so that no information is lost. The simplicity of the characteristic model based ACAC method makes it convenient for practical engineering applications.

This thesis explores the application of the characteristic model based all-coefficient adaptive

control method to the stabilization of a flexible rotor AMB system. Simulation has shown performance improvements over the μ-synthesis in terms of minimizing the vibration and maintaining a small orbit. Experimental results have also demonstrated some features of ACAC method and shown it is comparable to the μ-synthesis in certain measures. These results show its strong potential to perform well in spite of its simplicity.

Acknowledgments

I would like to thank Prof. Zongli Lin for providing me the opportunity to join ROMAC, supporting me to work on a new control method, encouraging me to be always pursuing excellence and be self-contained, spending enormous amount of time correcting my papers and my writing habit. Without his guidance and advices, this research would have progressed more slowly.

I would also like to thank Dr. Simon Mushi for helping me with his test rig, teaching me how to operate it, and answering my questions. It has been great to work with him and I really have learnt a lot. I also want to thank ROMAC fellow students and faculty members, Parinya, Dr. Se Young Yoon, Dr. Wei Jiang and Prof. Allaire, for sharing their knowledge and for discussing with me problems related to AMB and control so I can finish my learning curve in the least amount of time. When I have questions, they are always so helpful. Without their collaborations, I would not make such progress.

Finally, I want to thank Prof. Gang Tao and Dr. Timothy Dimond for serving as my committee members and supervising my research.

Contents

List of Figures

Chapter 1

Introduction

Active magnetic bearings have been an active research subject for decades and are becoming popular in practical applications. AMBs operate quite differently from conventional mechanical bearings. On one hand, AMBs rely on electromagnetic force to support the object. There is no physical contact, creating an operation environment nearly free of friction. On the other hand, AMBs require feedback control to generate appropriate supporting force, which demands additional electronics. Although AMBs possess several advantages such as high efficiency and reliability, low maintenance and repair costs, and clean working environment, they are also more complex since they require auxiliary equipment to provide the desired control performance. Because of the nonlinearity and open-loop instability of AMB systems, the controller design is the most essential task in an AMB application.

PID controllers are the most widely used control mechanism for magnetic bearing systems [4]. Because of their simplicity, PID controllers are easy to implement and can be tuned intuitively. They can achieve reasonable control performance after the tuning process. However, for complex dynamic systems, it is difficult for PID controllers to deliver robust performance. In recent years, robust control techniques such as μ-synthesis have also been applied to magnetic bearing applications [5, 6]. Compared with the PID control, the μ-synthesis approach is able to better handle the uncertainties in complex systems and to achieve better control performance. However, μ-synthesis requires accurate plant and uncertainty models to generate the most suitable solution, and in reality, it takes a lot of efforts to model a complex system. Besides, if the properties of the plant change significantly, the original μ controller might not work properly anymore [7].

The characteristic model based all-coefficient adaptive control (ACAC) method has been widely used in process control and aerospace industry, and numerous applications have demonstrated its effectiveness [8]. This method is able to provide robust control performance on multi-dimensional complex dynamical systems, while maintaining a simple structure and not requiring the actual plant model [9–11]. Motivated by its strong control performance and simplicity, in this thesis, we explore the application of the characteristic model based ACAC method on magnetic bearing systems.

1.1 Magnetic Bearings

Magnetic bearings were invented during World War II and became more mature and applicable for practical use around 25 years ago [12]. Magnetic bearing use electromagnetic force to pull the rotor with a mounted lamination stack from a ferromagnetic stator so that a certain clearance can be obtained. There are several poles on the stators, which are usually configured as 8 poles or 16 poles. Generally there exist two types of magnetic bearing designs. One is to handle the radial direction movement (radial bearings) and the other is to handle the axial direction movement (thrust bearings). A typical magnetic bearing is shown in Fig. 1.1. In this thesis, we will focus on the radial bearings.

Figure 1.1: An active magnetic bearing [1].

In order to achieve typical operational objectives, including levitation, minimization of rotor vibration, endurance and failsafe features, a complete rotor magnetic bearing system generally consists of

- Real time digital control system, such as DSP, FPGA, RT-linux,
- Data acquisition and real-time monitoring system, such as Labview,
- Hall position sensors, current transducers, optical probes, amplifiers and anti-aliasing filters,
- Auxiliary backup bearings,
- Backup power system,
- Rotor with lamination stacks, and
- Radial and/or thrust magnetic bearings.

The controller is the most essential element in an AMB system because magnetic bearings need feedback control to operate. Analog control systems were widely used in the early days and they were capable of handling simple AMB control applications. Because they could operate in real time and possess high control bandwidth, analog controllers are theoretically very effective. However, because the components in analog controllers are hard-wired, it is difficult to change the configurations and activate new functions. Besides, the resulting closed-loop system is sensitive to environmental changes and component aging. As a result, they cannot be operated under some extreme external conditions. Digital controllers have become more and more popular in AMB applications [13]. Digital controllers are implemented by digital signal processors (DSPs), which are powerful and flexible for control implementations. Compared with analog controllers, digital controllers are more compact and reliable, and they are less susceptible to the sensitivity issues.

When an AMB system is running, a variety of data need to be collected and monitored simultaneously, such as the orbit size of the shaft, the control voltage and current, and the running speed. DSP computers usually include functions for graphic user interface (GUI) designs so we can directly display the sensor data on the computer. Labview is another powerful data acquisition and monitoring system. Compared with the DSP built-in logging function, Labview is able to display the data at a higher sampling rate and in different forms by using the built-in transformation blocks. This allows to detect any failure and to thoroughly diagnose the system operating conditions.

Some other electrical components are also indispensable for the operation of an AMB system. The Hall effect probes measure the displacement of the shaft with respect to the geometric center,

which provides important feedback for the controller. The operational amplifiers convert the control voltage to current and two amplifiers are required for each control axis of a magnetic bearing. The current transducers measure how much control current goes through the coil and the optical probes read how fast the shaft is rotating. The anti-aliasing filters are used to restrict the bandwidth of a signal so when the signal is sent to the sampler, no aliasing will occur. A backup ball bearing is usually mounted on the stator and there is enough clearance between the magnetic bearing and the ball bearing. When the power is off, the ball bearing sustains the shaft and there is no contact with the magnetic bearing. If the shaft is running and suddenly the power is cut off, the ball bearing can absorb the impact from shaft dropping and protect the magnetic bearing and the rest of the machine.

Some advantages of magnetic bearing over conventional bearings are highlighted as follows:

- High energy efficiency,
- Low power consumption,
- Being nearly maintenance-free,
- Being free of lubrication,
- No mechanical wear,
- Allowing extreme working conditions, and
- High speed operations.

AMBs have been used in compressors, flywheel energy storage systems, machine tool spindles, and many other applications related to energy, oil and gas, and turbomachinery. Although the initial cost for those devices to use AMBs is higher than to use the conventional bearings due to the additional equipment, the advantages of efficiency and maintenance will compensate for the cost. In the long run, AMBs will show their strong potentials. AMB supported artificial heart pump is also getting more and more popular, where AMBs play a critical role. Because they do not require lubrication and their regular service is much easier than that of conventional bearings, there will not be contamination to human body and the patients do not need to suffer from frequent replacement of heart pump components. Some typical applications for AMBs are shown in Figs. 1.2 and 1.3.

Figure 1.2: Industrial compressor [2].

Figure 1.3: Gas turbine [3].

1.2 Fundamentals in AMB Control

AMB control systems modulate electromagnetic forces to stabilize rotor position. Here a one degree of freedom AMB model is used to illustrate the force characteristics. As shown in Fig. 1.4, the magnetic force can be calculated based on Ampere's Law and the conservation of magnetic flux as follows,

$$f = \frac{\mu_0 N^2 A_g I^2}{4 g_0^2}, \tag{1.1}$$

where μ_0 is the permeability, I is the current, N is the number of turns of wires, A_g is the face area of the pole and g_0 is the size of the air gap.

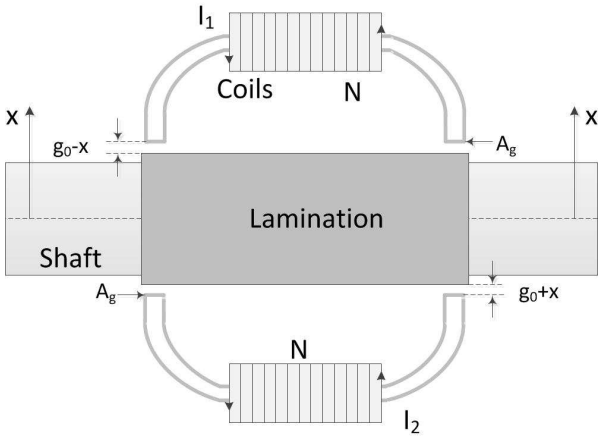

Figure 1.4: AMB control fundamental.

The net force generated by a pair of electromagnets based on the movement x and the air gap can be expressed as

$$f = f_1 - f_2 = \frac{\mu_0 N^2 A_g I_1^2}{4(g_0 - x)^2} - \frac{\mu_0 N^2 A_g I_2^2}{4(g_0 + x)^2} = \frac{\mu_0 N^2 A_g}{4}\left[\frac{I_1^2}{(g_0 - x)^2} - \frac{I_2^2}{(g_0 + x)^2}\right]. \tag{1.2}$$

The currents I_1 and I_2 are based on the bias current I_b and the perturbation i generated from the controller as

$$I_1 = I_b + i, \qquad I_2 = I_b - i. \tag{1.3}$$

Then, the force equation can be written as

$$f = \frac{\mu_0 N^2 A_g}{4}\left[\frac{I_1^2}{(g_0 - x)^2} - \frac{I_2^2}{(g_0 + x)^2}\right] = \frac{\mu_0 N^2 A_g}{4}\left[\frac{4I_b^2 g_0 x + 4i^2 g0x + 4I_b i g_0^2 + 4I_b i x^2}{(g_0^4 + x^4 - 2g_0^2 x^2)}\right]. \tag{1.4}$$

Linearization of the expression in (1.4) around the equilibrium point ($i = 0$ and $x = 0$) results in

$$f = \frac{\mu_0 N^2 A_g}{g_0^4}(I_b^2 g_0 x + I_b i g_0^2) = \frac{\mu_0 N^2 A_g I_b^2}{g_0^3} x + \frac{\mu_0 N^2 A_g I_b}{g_0^2} i, \tag{1.5}$$

$$f = k_x x + k_i i, \tag{1.6}$$

where $k_x = \frac{\mu_0 N^2 A_g I_b^2}{g_0^3}$ and $k_i = \frac{\mu_0 N^2 A_g I_b}{g_0^2}$ are the stiffness and current gains.

Because of the negative stiffness generated by the magnetic force, AMB is inherently unstable. More than one channel always need to be controlled, so the multiple-input multiple-output (MIMO) control design strategy can usually facilitate the task. As shown in Fig. 1.5, for a magnetic bearing with 8 poles, each axis needs a pair of amplifiers and a total of four amplifiers are required to provide currents to the coils. The controller will produce suitable control voltages to the amplifiers based on the measurements of position sensors, where two sensors are mounted for each axis. After the magnetic forces are applied to the shaft, the shaft can be levitated with a specified clearance.

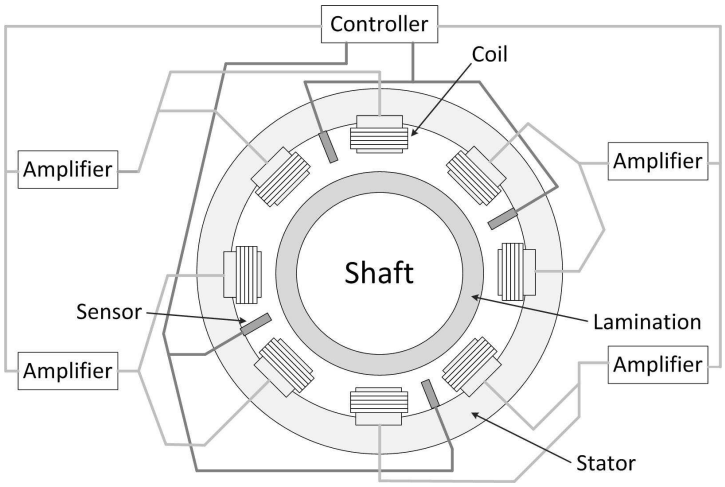

Figure 1.5: Basic AMB control components.

1.3 Review of AMB Control Literature

AMB systems have the capability of compensating for vibration forces and keeping the shaft near the geometry axis within the limits of the actuator capacity and bandwidth. For AMB supported rotors, currently there are several general methods to deal with vibration minimization. Automatic balancing control [14] is a typical strategy for cancelation and rejection of the synchronous bearing reaction force. There is also adaptive unbalance control [15], which can reduce the bearing reaction force and housing vibration. These approaches aim to reduce the synchronous component of the rotor response to the amplifier. However, these approaches usually cannot deal with bending critical speeds so they cannot be directly applied to flexible rotors. The second category for cancelation and rejection of unbalance vibrations includes periodic learning control [16] and real time balancing

[17]. These approaches aim to reduce the measured rotor position error. They can minimize the vibration induced by unbalance with appropriate compensation generated in AMBs and are suitable for precise position control applications. The third category aims to deal with the bending modes, including optimum damping control [18] and synchronous vibration control [19]. These strategies can attenuate the vibration when the rotor passes through bending critical speeds. If there exists a large residual unbalance, a large amplifier power for large magnetic bearing compensation force is needed.

For a flexible rotor, because of its bending natural modes, it has higher gain near those natural frequencies and it also has a wider mechanical bandwidth than a regular rigid rotor, which brings control bandwidth issues. The controller needs to have excellent dynamic performance at high frequency to control a flexible rotor. Besides those, the sensor and actuator noncollocation is also an important issue because around bending critical speeds, the sensor measurement could be different from the actual shaft movement at the bearing. Generally there are two approaches to deal with bending flexible modes, one is called phase compensation and the other is called gain compensation [4]. For the phase compensation, the phase of the controller should be positive near the bending frequency and the gain product of the controller and plant should be bigger than 1. For the gain compensation, the gain product of the controller and plant should be less than 1 even though the controller could have negative phase near the bending frequency. The controller usually needs to combine both approaches to achieve stability and performance requirements.

Control of flexible rotors supported by AMBs have been reported on by several researchers [6, 20–23]. Several PID control designs have been documented in controlling flexible high speed rotors. In general, a PID controller itself could not stabilize the flexible modes, so notch filters are needed. Besides, low-pass filters are necessary to roll off the control signal at high frequencies so the noise is not amplified. In some of the literature, additional filters such as the phase bump filter were proposed to enhance the performance of PID control [22]. Robust control μ synthesis has also been applied to control of flexible rotors and good results have been documented [6, 20]. The μ controller does not need any additional filters and the inherent notch effect makes it ideal to handle flexible modes. It provides robust stability and performance under certain ranges of parameter variations so it is quite reliable for AMB control applications.

1.4 Objectives of the Thesis

The main goal of this thesis is to explore using the characteristic model based ACAC method to stabilize a flexible rotor AMB test rig. The new control method will be compared with an existing μ-synthesis controller in both simulations and experiments so we can fully understand its advantages and limitations.

1.5 Organization of the Thesis

The thesis is organized as follows: Chapter 2 presents the all-coefficient adaptive control. First this method is briefly introduced, then we will study the golden-section robust control method and analyze it with stable and unstable second order systems. Afterwards, the golden-section adaptive control is described and some simulation results are shown at the end. Chapter 3 presents the characteristic modeling. First it is applied to a linear time-invariant plant with only distinct nonzero poles, then it is applied to a linear time-invariant plant with additional zero poles and repeated real poles. Afterwards, the characteristic modeling method is analyzed and the modeling error issue is addressed. At the end of this chapter, some simulation results are presented. Chapter 4 presents the application of the characteristic model based all-coefficient adaptive control to an AMB system. First it describes the flexible rotor AMB test rig and an existing μ-synthesis controller, then the concept of characteristic modeling with all-coefficient adaptive control mechanism is introduced. Afterwards, it applies the characteristic modeling method to the rotor AMB model and then it presents the implementation on the actual test rig and shows the simulation and experimental results. Conclusions and future work are summarized in Chapter 5.

Chapter 2

All-coefficient Adaptive Control

All-coefficient adaptive control (ACAC) was originally developed by Wu and his colleagues in the 1980's [24]. It aims to resolve many practical engineering problems more effectively than the conventional adaptive control. It can be easily implemented and applied to many engineering systems for control operations [25, 26].

The early development of ACAC focused on linear time-invariant plants with unknown plant parameters. It was later discovered that ACAC could also be applied to linear slowly time-varying systems and certain nonlinear systems. One of the most important conclusions in the development of ACAC is that under the proposed circumstances, the sum of all the coefficients from the derived discretized system equal to one. Based on this condition, the selection of the initial values of system coefficients gets simplified and it reduces the calculation for parameter estimations. Besides, it can guarantee the boundness of the controller coefficients by using the least-squares parameter estimation algorithm. The ACAC method also plays an important role in the characteristic model based intelligent control theory and the golden-section controller is based on the ACAC method. By combining the characteristic modeling and golden-section adaptive control, it formulates a complete system modeling and control design method.

The ACAC method guarantees not only the closed-loop stability but also sufficient performance during the transient process. The golden-section adaptive controller is one of the most important components in the all-coefficient adaptive control structure. It will be demonstrated that this controller design can deliver good dynamic performance and make the closed-loop system stable when the sampling time satisfies certain conditions.

In this chapter, we will summarize the ACAC method and the golden-section control design.

2.1 All-coefficient Adaptive Control Method

Consider a linear time-invariant plant described by the following differential equation

$$y^{(n)} = a_{n-1}y^{(n-1)} + \cdots + a_0 y + b_{m-1}u^{(m-1)} + \cdots + b_0 u, \tag{2.1}$$

where $n > m$. The discretized form of (2.1) is given as

$$y(k+n) = \alpha_1 y(k+n-1) + \cdots + \alpha_n y(k) + \beta_0 u(k+m-1) + \cdots + \beta_{m-1}u(k), \tag{2.2}$$

with the transfer function

$$G(z) = \frac{Y(z)}{U(z)} = \frac{\beta_0 z^{m-1} + \beta_1 z^{m-2} + \cdots + \beta_{m-1}}{z^n - \alpha_1 z^{n-1} - \alpha_2 z^{n-2} - \cdots - \alpha_n}. \tag{2.3}$$

The coefficients of Eq. (2.2) satisfy the following conditions [8]:

- If the static gain D equals to unity, where $D = -b_0/a_0$, then the sum of all the coefficients equals to one, *i.e.*,

$$\sum_{i=1}^{n} \alpha_i + \sum_{i=0}^{m-1} \beta_i = 1.$$

- If the static gain $D \neq 0$ and is bounded, the sum of all the coefficients approaches one as the sampling time $T \to 0$, *i.e.*,

$$\lim_{T\to 0} \left(\sum_{i=1}^{n} \alpha_i + \sum_{i=0}^{m-1} \beta_i \right) = 1.$$

When $T \to 0$, we have the following approximations:

$$\begin{aligned}
\left.\frac{dy(t)}{dt}\right|_{t=KT} &= \frac{y(k+1)-y(k)}{T} = \frac{\sum_{i=0}^{1} p_{1,i}y(k+i)}{T};\\
\left.\frac{dy^2(t)}{dt^2}\right|_{t=KT} &= \frac{y(k+2)-2y(k+1)+y(k)}{T^2} = \frac{\sum_{i=0}^{2} p_{2,i}y(k+i)}{T^2};\\
&\vdots\\
\left.\frac{dy^n(t)}{dt^n}\right|_{t=KT} &= \frac{y(k+n)+\sum_{i=0}^{n-1} c_i y(k+i)}{T^n} = \frac{\sum_{i=0}^{n} p_{n,i}y(k+i)}{T^n}.
\end{aligned} \tag{2.4}$$

$$\begin{aligned}
\left.\frac{du(t)}{dt}\right|_{t=KT} &= \frac{u(k+1)-u(k)}{T} = \frac{\sum_{j=0}^{1} q_{1,j}u(k+j)}{T};\\
\left.\frac{du^2(t)}{dt^2}\right|_{t=KT} &= \frac{u(k+2)-2u(k+1)+u(k)}{T^2} = \frac{\sum_{j=0}^{2} q_{2,j}u(k+j)}{T^2};\\
&\vdots\\
\left.\frac{du^{m-1}(t)}{dt^{m-1}}\right|_{t=KT} &= \frac{u(k+m-1)+\sum_{j=0}^{m-2} d_j u(k+j)}{T^{m-1}} = \frac{\sum_{j=0}^{m-1} q_{m-1,j}u(k+j)}{T^{m-1}}.
\end{aligned}$$

It can be observed that $\sum_{i=0}^{n-1} c_i = -1$ and the sum of all the coefficients $\sum_{i=0}^{1} p_{1,i} = 0, \ldots, \sum_{i=0}^{n} p_{n,i} = 0$, $\sum_{j=0}^{1} q_{1,j} = 0, \ldots, \sum_{j=0}^{m-1} q_{m-1,j} = 0$ in Eq. (2.4). Substituting Eq. (2.4) in Eq. (2.1) results in

$$\begin{aligned}
y(k+n) = {} & a_{n-1}T\sum_{i=0}^{n-1} p_{n-1,i}y(k+i) + \cdots + a_1 T^{n-1}\sum_{i=0}^{1} p_{1,i}y(k+i)\\
& + a_0 T^n y(k) + b_{m-1}T^{n-m+1}\sum_{j=0}^{m-1} q_{m-1,j}u(k+j) + \cdots + b_1 T^{n-1}\sum_{j=0}^{1} q_{1,j}u(k+j)\\
& + b_0 T^n u(k) - \sum_{i=0}^{n-1} c_i y(k+i),
\end{aligned}$$

which is in the form of Eq. (2.2). Thus,

$$\sum_{i=1}^{n}\alpha_i+\sum_{j=0}^{m-1}\beta_j=a_0T^n+b_0T^n-\sum_{i=0}^{n-1}c_i. \tag{2.5}$$

Since $\sum_{i=0}^{n-1}c_i=-1$, we have $\sum_{i=1}^{n}\alpha_i+\sum_{j=0}^{m-1}\beta_j=1$ as $T\to 0$.

When the static gain $D=-b_0/a_0$, the coefficients of the difference equation above follow

$$\sum_{i=1}^{n}\alpha_i+(-\frac{a_0}{b_0})\sum_{i=0}^{m-1}\beta_i=\sum_{i=1}^{n}\alpha_i+\frac{1}{D}\sum_{i=0}^{m-1}\beta_i=1,$$

because $D=\frac{\beta_0+\beta_1+\cdots+\beta_{m-1}}{1-\alpha_1-\alpha_2-\cdots-\alpha_n}$ for $z=1$ based on Eq. (2.3).

Therefore, $\sum_{i=1}^{n}\alpha_i+\sum_{i=0}^{m-1}\beta_i=1$ when $D=-b_0/a_0=1$.

Based on the derivation above, several extended conclusions can be acquired:

- When $a_0=0$ in Eq. (2.1), it can be easily observed that for Eq. (2.2)

$$\sum_{i=1}^{n}\alpha_i=1.$$

- When $a_0\neq 0$, it can be observed that

$$a_0=-\prod_{i=1}^{n}p_i=-\prod_{i=1}^{n}\frac{1}{T_i},$$
$$T^{'}=\sqrt[n]{\prod_{i=1}^{n}T_i},$$

  where p_i are the poles of the transfer function derived from Eq. (2.1), T_i are the time constants for each pole and it can be derived that $a_0=-(\frac{1}{T'})^n$.

- Although the values of a_0 and $T^{'}$ are unknown, it is not difficult to find the possible maximum value of $|a_0|$ or the ranges of the maximum pole $|p_{i\,\max}|$ [27], so we can define the minimum

equivalent time constant $T_{\min}$ and the the maximum equivalent time constant $T_{\max}$ as follows,

$$T_{\min} = \sqrt[n]{\frac{1}{\prod_{i=1}^{n} |p_{i\max}|}} = \sqrt[n]{\frac{1}{|a_{0\max}|}},$$
$$T_{\max} = \sqrt[n]{\frac{1}{\prod_{i=1}^{n} |p_{i\min}|}} = \sqrt[n]{\frac{1}{|a_{0\min}|}}.$$

- When the system static gain equals to 1, no matter how big the sampling time T is chosen, the sum of the coefficients will be equal to 1. When the static gain does not equal to 1 but T approaches 0, the sum of the coefficients also approaches 1. When $D \neq 1$ and $T \not\to 0$, $\sum_{i=1}^{n} \alpha_i + \sum_{j=0}^{m-1} \beta_j = 1 + \varepsilon$ and $\varepsilon = (D-1)(\frac{T}{T'})^n$.

The ranges of α_i and β_i can be determined in advance based on the ranges of a_i and b_i. The sampling time T is usually chosen as

$$T \leq \frac{T_{\min}}{15}.$$

Once the ranges of the parameters are specified, parameter estimates should not only rely on the parameter estimation algorithm, but also satisfy the requirements that they are constrained by closed sets and the sum of all the coefficients should be equal to one. The initial values of those coefficients are chosen from the specified closed sets, so the estimated parameters can be closer to their real values, which will improve the performance of the adaptive control during the transient process.

The difference equation (2.2) can be parameterized in the following compact form,

$$y(k) = \phi^T(k)\theta + \beta_0 u(k), \tag{2.6}$$

where $\phi(k)$ and θ are defined as

$$\phi(k) = [y(k-1)\ \ y(k-2)\ \ \cdots\ \ y(k-n)\ \ u(k-1)\ \ u(k-2)\ \ \cdots\ \ u(k-m+1)]^T,$$
$$\theta = [\alpha_1\ \ \alpha_2\ \ \cdots\ \ \alpha_n\ \ \beta_1\ \ \beta_2\ \ \cdots\ \ \beta_{m-1}]^T.$$

The feedback control $u(k)$ is given as

$$u(k) = -\phi^T(k)L(k),$$

where $L(k) = [L_1(k) \quad L_2(k) \cdots L_{2n-1}(k)]$ is the feedback gain that satisfies the conditions of making the system (2.6) stable.

We can adopt a least-squares algorithm to update $\hat{\theta}(k)$ as follows [24],

$$\begin{aligned}
P(k)=&P(k-1)-\frac{P(k-1)\phi(k)\phi^T(k)P(k-1)}{\lambda+\phi^T(k)P(k-1)\phi(k)},\\
\hat{\theta}(k)=&\hat{\theta}(k-1)+\beta_0(k)L(k)-\beta_0(k-1)L(k-1)\\
&+P(k)\phi(k)[y(k)-\phi^T(k)(\hat{\theta}(k-1)-\beta_0(k-1)L(k-1))].
\end{aligned}$$

Also, based on the fact that the sum of all the coefficients equals to 1, it follows that [24], the coefficient $\hat{\beta}_0$ can be updated as follows

$$\hat{\beta}_0(k) = \hat{\beta}_0(k-1)-\frac{\theta_s+\hat{\beta}_0(k-1)-1}{L_s+1}-MP(k)\phi(k)\frac{y(k)-\phi(k)^T[\hat{\theta}(k-1)-\hat{\beta}_0(k-1)L(k)]}{L_s+1},$$

where θ_s, L_s and M are given as

$$\begin{aligned}
\theta_s &= \sum_{i=1}^{2n-1}\theta_i(k-1),\\
L_s &= \sum_{j=1}^{2n-1}L_j(k),\\
M &= [\underbrace{1\ 1\cdots 1}_{2n-1}\ \underbrace{0\ 0\cdots 0}_{n}].
\end{aligned}$$

The general all-coefficient adaptive control $u(k)$ consists of a maintaining/tracking control $u_m(k)$, a golden-section feedback control $u_f(k)$, a logic differential control $u_d(k)$ and a logic integral control $u_i(k)$ [8]. It can be written as

$$u(k) = u_m(k) + u_f(k) + u_d(k) + u_i(k),$$

where $u_m(k)$, $u_f(k)$, $u_d(k)$ and $u_i(k)$ are respectively specified as

1. Maintaining/tracking control

$$u_m(k) = \frac{y_r(k) - \phi^T(k)\hat{\theta}(k)}{\hat{\beta}_0(k)},$$

where $y_r(k)$ is the desired output;

2. Golden-section feedback control

$$u_f(k) = \frac{l_1\hat{\alpha}_1(k)\tilde{y}(k) + l_2\hat{\alpha}_2(k)\tilde{y}(k-1)}{\hat{\beta}_0(k)},$$

where $l_1 = 0.382$, $l_2 = 0.618$, $\hat{\alpha}_1(k)$ and $\hat{\alpha}_2(k)$ are the estimates of α_1 and α_2, and $\tilde{y}(k) = y_r(k) - y(k)$;

3. Logical differential control

$$u_d(k) = k_1\frac{\tilde{y}(k) - \tilde{y}(k-1)}{T},$$
$$k_1 = k_d\sqrt{\sum_{i=1}^{N}[|\ \tilde{y}(k-N+i) - \tilde{y}(k-N+i-1)\ |]}\ ,$$

where k_d is a positive constant;

4. Logical integral control

$$u_i(k) = u_i(k-1) + k_2\tilde{y}(k),$$
$$k_2 = \begin{cases} k_{i1}, & \tilde{y}(k)[\tilde{y}(k) - \tilde{y}(k-1)] - \psi \leq 0, \\ k_{i2}, & \tilde{y}(k)[\tilde{y}(k) - \tilde{y}(k-1)] - \psi > 0, \end{cases}$$

where k_{i2}, k_{i1} and ψ are all positive constants with $k_{i2} > k_{i1}$ and ψ being a small number.

2.2 Golden-section Robust Control Method

The golden-section robust controller is based on the all-coefficient adaptive control theory. This method brings the golden-section ratio ($l_1/l_2 = 0.382/0.618$) into the controller design. The golden-section adaptive control aims to effectively control systems with unknown parameters. It is able to make the closed-loop system stable with a simple control structure and it is very robust [28]. In this

section, we will introduce the golden-section robust controller and analyze the closed-loop system stability with a second order system.

Consider a dynamic system that can be described by the following second order differential equation

$$\ddot{y}(t) + a_1\dot{y}(t) + a_0 y(t) = b_1\dot{u}(t) + b_0 u(t), \tag{2.7}$$

whose transfer function is given as follows,

$$G(s) = \frac{Y(s)}{U(s)} = \frac{b_1 s + b_0}{s^2 + a_1 s + a_0} = \frac{k_1}{s + p_1} + \frac{k_2}{s + p_2}, \tag{2.8}$$

where $k_1 = \frac{b_0 - \frac{a_1 - \sqrt{a_1^2 - 4a_0}}{2} b_1}{\sqrt{a_1^2 - 4a_0}}$, $k_2 = \frac{-b_0 + \frac{a_1 + \sqrt{a_1^2 - 4a_0}}{2} b_1}{\sqrt{a_1^2 - 4a_0}}$, $p_1 = \frac{a_1 - \sqrt{a_1^2 - 4a_0}}{2}$, and $p_2 = \frac{a_1 + \sqrt{a_1^2 - 4a_0}}{2}$. Here we have assumed that $p_1 \neq p_2$.

Discretization of $G(s)$ with a zero order hold results in

$$\begin{aligned} G(z) &= Z\left[\frac{1 - e^{-sT}}{s}\frac{k_1}{s + p_1}\right] + Z\left[\frac{1 - e^{-sT}}{s}\frac{k_2}{s + p_2}\right] \\ &= \frac{[k_1 T_{\max}(1 - e^{-T/T_{\max}}) + k_2 T_{\min}(1 - e^{-T/T_{\min}})]z^{-1}}{1 - (e^{-T/T_{\min}} + e^{-T/T_{\max}})z^{-1} + e^{-T/T_{\min}} e^{-T/T_{\max}} z^{-2}} \\ &\quad + \frac{[k_1 T_{\max}(e^{-T/T_{\max} - T/T_{\min}} - e^{-T/T_{\min}}) + k_2 T_{\min}(e^{-T/T_{\max} - T/T_{\min}} - e^{-T/T_{\max}})]z^{-2}}{1 - (e^{-T/T_{\min}} + e^{-T/T_{\max}})z^{-1} + e^{-T/T_{\min}} e^{-T/T_{\max}} z^{-2}}, \end{aligned} \tag{2.9}$$

where $T_{\max} = 1/p_1$ and $T_{\min} = 1/p_2$.

The discrete-time version of Eq. (2.7) can be written as

$$y(k+2) = \alpha_1 y(k+1) + \alpha_2 y(k) + \beta_0 u(k+1) + \beta_1 u(k), \tag{2.10}$$

and its transfer function can be obtained as follows,

$$\frac{Y(z)}{U(z)} = \frac{\beta_0 z + \beta_1}{z^2 - \alpha_1 z - \alpha_2} = \frac{\beta_0 z^{-1} + \beta_1 z^{-2}}{1 - \alpha_1 z^{-1} - \alpha_2 z^{-2}}. \tag{2.11}$$

Comparing Eq. (2.9) with Eq. (2.11), we can find:

$$\alpha_1 = e^{-T/T_{\min}} + e^{-T/T_{\max}}, \quad \alpha_2 = -e^{-T/T_{\min}-T/T_{\max}},$$
$$\beta_0 = k_1 T_{\max}(1 - e^{-T/T_{\max}}) + k_2 T_{\min}(1 - e^{-T/T_{\min}}),$$
$$\beta_1 = k_1 T_{\max}(e^{-T/T_{\max}-T/T_{\min}} - e^{-T/T_{\min}}) + k_2 T_{\min}(e^{-T/T_{\max}-T/T_{\min}} - e^{-T/T_{\max}}).$$

Let the ratio between the sampling time and the minimum equivalent time constant $\eta = \frac{T}{T_{\min}}$ satisfy $\eta \in [0, \eta_{\max}]$ and the ratio between the sampling time and the maximum equivalent time constant satisfies $\frac{T}{T_{\max}} \in [0, \frac{T}{T_{\min}}]$. For a second order system,

$$\alpha_1 \in [2e^{-T/T_{\min}}, 2e^{-T/T_{\max}}],$$
$$\alpha_2 \in [-e^{-2T/T_{\max}}, -e^{-2T/T_{\min}}].$$

Assuming the plant is stable, then, by the Jury Test, we have

$$|\alpha_2| < 1, \tag{2.12}$$
$$1 - \alpha_1 - \alpha_2 > 0, \tag{2.13}$$
$$1 + \alpha_1 - \alpha_2 > 0. \tag{2.14}$$

Therefore, $-1 < \alpha_2 < 1$, $\alpha_1 + \alpha_2 < 1$, $\alpha_2 - \alpha_1 < 1$. For stable plants, it has been established in [29] for the following results:

$$\begin{cases} 2e^{-\eta_{\max}} \leq \alpha_1 \leq 2, \\ -1 < \alpha_2 \leq -e^{-2\eta_{\max}}, \\ 2e^{-\eta_{\max}} - e^{-2\eta_{\max}} < \alpha_1 + \alpha_2 \leq 1, \\ \frac{b_0 T^2}{2}\left(1 - \frac{2\eta_{\max}}{3}\right) < \beta_0 < \frac{b_0 T^2}{2}, \\ \frac{b_0 T^2}{2}\left(1 - \frac{4\eta_{\max}}{3} - \frac{5\eta_{\max}^2}{6}\right) < \beta_1 < \frac{b_0 T^2}{2}\left(1 - \frac{\eta_{\max}^2}{24}\right), \end{cases} \tag{2.15}$$

and for unstable plants, according to [29],

$$\begin{cases} 2\cos(\frac{\eta_{\max}}{2}) \leq \alpha_1 \leq 2e^{\frac{\eta_{\max}}{2}}, \\ -e^{\eta_{\max}} < \alpha_2 \leq -1, \\ 2e^{\frac{\eta_{\max}}{2}}\cos(\frac{\eta_{\max}}{2}) - e^{\eta_{\max}} \leq \alpha_1 + \alpha_2 < 1, \\ \frac{b_0 T^2}{2} < \beta_0 < \frac{b_0 T^2}{2}\left(1 + \frac{\eta_{\max}}{3} + \frac{\eta_{\max}^2}{12}\right), \\ \frac{b_0 T^2}{2}\left(1 - \frac{\eta_{\max}^2}{24}\right) < \beta_1 < \frac{b_0 T^2}{2}\left(1 + \frac{2\eta_{\max}}{3} + \frac{7\eta_{\max}^2}{24}\right). \end{cases} \tag{2.16}$$

The definition of the minimum equivalent time constant can be specified as follows according to the poles in Eq. (2.8):

- If p_1 and p_2 are real poles, $p_1 \leq p_2 < 0$ or $p_1 < p_2 \leq 0$, the minimum equivalent time constant $T_{\min} = -\frac{1}{p_1}$;
- If p_1 and p_2 are real poles, $0 < p_1 \leq p_2$, $T_{\min} = \frac{1}{2p_2}$;
- If p_1 and p_2 are real poles, $p_1 < 0 < p_2$, $T_{\min} = \min\left[-\frac{1}{2p_1}, \frac{1}{2p_2}\right]$;
- If p_1 and p_2 are complex conjugate poles, $p_1 = \sigma + j\omega$, $p_2 = \sigma - j\omega$, $T_{\min} = \min\left[-\frac{1}{|2\sigma|}, \frac{1}{|2\omega|}\right]$ for $\sigma \neq 0$, $T_{\min} = \frac{1}{|2\omega|}$ for $\sigma = 0$.

Now we need to summarize the ranges of α_1, α_2, β_0 and β_1. For stable plants, based on Eq. (2.15), it can be observed that $\alpha_1 \to 2$, $\alpha_2 \to -1$, $\beta_0 \to 0$, $\beta_1 \to 0$ as $T \to 0$. From a practical point of view,

$$\begin{cases} \frac{T}{T_{\min}} \in [\frac{1}{10}, \frac{1}{3}], \\ \frac{T}{T_{\max}} \in [0, \frac{1}{10}]. \end{cases}$$

For practical systems, β_1 can be ignored [29]. When $\eta_{\max} \leq \frac{1}{3}$, $\beta_0 = \frac{b_0}{a_0}(\frac{T}{T_{\min}})^2$, $\frac{b_0}{a_0} = D \in (0.3, 3)$, the ranges of α_1, α_2 and β_0 can be calculated as

$$N_1 = \begin{cases} \alpha_1 \in [1.4331, 1.9975], \\ \alpha_2 \in [-1, -0.5134], \\ \alpha_1 + \alpha_2 \in [0.9196, 1], \\ \beta_0 \in [0.003, 0.3]. \end{cases}$$

Based on Eq. (2.16), for unstable plants, it can be observed that $\alpha_1 \to 2$, $\alpha_2 \to -1$, $\beta_0 \to 0$, $\beta_1 \to 0$ as $T \to 0$. Let

$$\begin{cases} \frac{T}{T_{\min}} \in [\frac{1}{10}, \frac{1}{4}], \\ \frac{T}{T_{\max}} \in [0, \frac{1}{10}]. \end{cases}$$

Then the ranges for the corresponding parameters can be calculated with $\eta_{\max} \leq \frac{1}{4}$ and $D \in (0.3, 3)$ [24],

$$N_2 = \begin{cases} \alpha_1 \in [1.9844, 2.2663], \\ \alpha_2 \in [-1.2840, -1], \\ \alpha_1 + \alpha_2 \in [0.9646, 1], \\ \beta_0 \in [0.00075, 0.047]. \end{cases}$$

- For case when $p_1 < p_2 = 0$, the minimum equivalent time constant $T_{\min} = -\frac{1}{p_1}$, $\eta = -p_1 T$,

$$\begin{cases} \alpha_1 = e^{-\eta} + 1, \\ \alpha_2 = -e^{-\eta}, \\ \alpha_1 + \alpha_2 = 1. \end{cases}$$

- For case when $p_1 = p_2 = 0$,

$$\begin{cases} \alpha_1 = 2, \\ \alpha_2 = -1, \\ \alpha_1 + \alpha_2 = 1. \end{cases}$$

2.2.1 Golden-section robust control for stable second order systems

Since a second order system is closely related to the characteristic modeling method and the ranges of the system parameters have been specified, we will analyze the closed-loop stability of a second order linear time-invariant (LTI) system under the golden-section robust control. A stable system with unknown parameters is described as [29]

$$y(k+2) = \alpha_1 y(k+1) + \alpha_2 y(k) + \beta_0 u(k+1), \tag{2.17}$$

and the controller has the following structure

$$u(k) = y_r(k+1)/\hat{\beta}_0 - [l_1\hat{\alpha}_1 y(k) + l_2\hat{\alpha}_2 y(k-1)]/\hat{\beta}_0, \tag{2.18}$$

whose parameters are chosen from set N_1, so $\hat{\alpha}_1 \in [1.4331, 1.9975]$, $\hat{\alpha}_2 \in [-1, -0.5134]$ and $\hat{\beta}_0 \in [0.003, 0.3]$.

According to [30], $l_1 = 1$ and $l_2 = 1$ for a general form adaptive controller. Since we are trying to verify the golden-section robust control method, we will assume $0 < l_1 \leq 1$, $0 < l_2 \leq 1$.

Substituting Eq. (2.18) into (2.17), we have

$$y(k+2) = \left(\alpha_1 - \frac{\beta_0}{\hat{\beta}_0} l_1\hat{\alpha}_1\right) y(k+1) + \left(\alpha_2 - \frac{\beta_0}{\hat{\beta}_0} l_2\hat{\alpha}_2\right) y(k) + \frac{\beta_0}{\hat{\beta}_0} y_r(k+2). \tag{2.19}$$

The transfer function of the closed-loop system (2.19) can be obtained as follows,

$$\frac{Y(z)}{R(z)} = \frac{\frac{\beta_0}{\hat{\beta}_0} z^2}{z^2 + \left(\frac{\beta_0}{\hat{\beta}_0} l_1\hat{\alpha}_1 - \alpha_1\right) z + \left(\frac{\beta_0}{\hat{\beta}_0} l_2\hat{\alpha}_2 - \alpha_2\right)}, \tag{2.20}$$

and the characteristic equation is given as

$$z^2 + \left(\frac{\beta_0}{\hat{\beta}_0} l_1 \hat{\alpha}_1 - \alpha_1\right) z + \left(\frac{\beta_0}{\hat{\beta}_0} l_2 \hat{\alpha}_2 - \alpha_2\right) = 0. \tag{2.21}$$

Based on the Jury Test, the closed-loop system is stable if

$$\left|\frac{\beta_0}{\hat{\beta}_0} l_2 \hat{\alpha}_2 - \alpha_2\right| < 1, \tag{2.22}$$

$$1 + \left(\frac{\beta_0}{\hat{\beta}_0} l_1 \hat{\alpha}_1 - \alpha_1\right) + \left(\frac{\beta_0}{\hat{\beta}_0} l_2 \hat{\alpha}_2 - \alpha_2\right) > 0, \tag{2.23}$$

$$1 - \left(\frac{\beta_0}{\hat{\beta}_0} l_1 \hat{\alpha}_1 - \alpha_1\right) + \left(\frac{\beta_0}{\hat{\beta}_0} l_2 \hat{\alpha}_2 - \alpha_2\right) > 0. \tag{2.24}$$

From Eqs. (2.22) to (2.24), according to the coefficient ranges specified in the set N_1 and $0 < \frac{\beta_0}{\hat{\beta}_0} \leq 2$ [29], the following conditions can be derived to keep the closed-loop system stable:

$$l_2 < 1.9196 l_1, \tag{2.25}$$

$$l_2 < 1.45 - 2 l_1, \tag{2.26}$$

$$l_2 > 0. \tag{2.27}$$

Therefore, the values of l_1 and l_2 satisfying the conditions above must lie in the triangle defined by Eqs. (2.25), (2.26) and (2.27).

When $\hat{\alpha}_1 = \alpha_1$, $\hat{\alpha}_2 = \alpha_2$ and $\hat{\beta}_0 = \beta_0$, the characteristic equation of the closed-loop system becomes

$$z^2 + (l_1 - 1)\alpha_1 z + (l_2 - 1)\alpha_2 = 0. \tag{2.28}$$

Note that $\alpha_1 = e^{-T/T_{\min}} + e^{-T/T_{\max}}$, $\alpha_2 = -e^{-T/T_{\min}} e^{-T/T_{\max}}$, the open-loop poles $z_{o1} = e^{-T/T_{\min}}$ and $z_{o2} = e^{-T/T_{\max}}$. If $l_2 = 1 - (1 - l_1)^2$, the closed-loop poles have the following relations with z_{o1}

and z_{o2}:

$$z_{c1} = \frac{-(l_1-1)\alpha_1 + \sqrt{(l_1-1)^2\alpha_1^2 - 4(l_2-1)\alpha_2}}{2} = (1-l_1)z_{o1}, \tag{2.29}$$

$$z_{c2} = \frac{-(l_1-1)\alpha_1 - \sqrt{(l_1-1)^2\alpha_1^2 - 4(l_2-1)\alpha_2}}{2} = (1-l_1)z_{o2}. \tag{2.30}$$

For stable systems, $|z_{o1}| < 1$ and $|z_{o2}| < 1$, therefore,

$$|z_{c1}| < (1-l_1), \tag{2.31}$$

$$|z_{c2}| < (1-l_1). \tag{2.32}$$

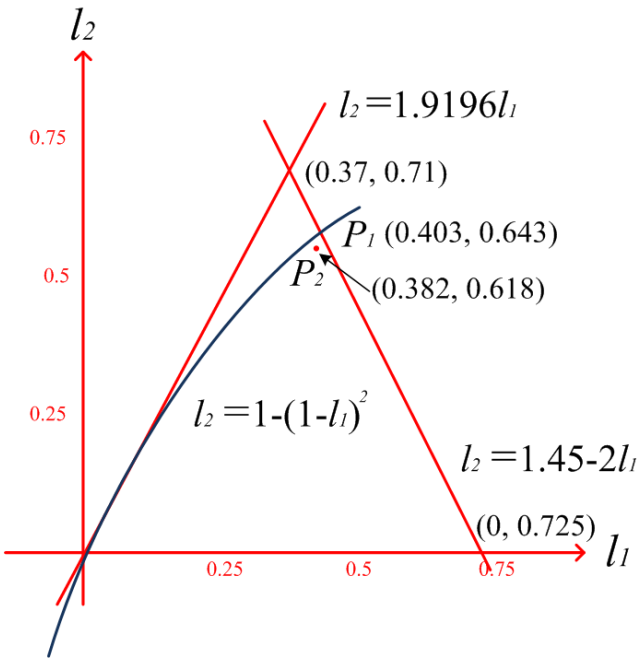

Figure 2.1: Parameter graph for a stable second order system.

If we use the relation $l_2 = 1-(1-l_1)^2$ and combine it with the triangle enclosed by Eqs. (2.25), (2.26) and (2.27), some important relations can be obtained based on Fig. 2.1. At point P_1, which is the intersection of $l_2 = 1-(1-l_1)^2$ and $l_2 = 1.9196l_1$, $l_1 = 0.403$, $l_2 = 0.643$. Because we know any combination of l_1 and l_2 in the triangle can make the system closed-loop stable, we can directly adopt the values of l_1 and l_2 at point P_1 while preserving some stability margin. Therefore,

$l_1 + l_2 = 0.403 + 0.643 = 1.046 \approx 1$ and we can obtain l_1 and l_2 with $l_2 = 1 - (1 - l_1)^2$:

$$l_1 = \frac{3 - \sqrt{5}}{2} = 0.382, \tag{2.33}$$

$$l_2 = \frac{\sqrt{5} - 1}{2} = 0.618. \tag{2.34}$$

It can be observed that at the point P_2, l_1 and l_2 satisfy the golden-section ratio and the closed-loop system is stable.

2.2.2 Golden-section robust control for unstable second order systems

We now consider an unstable second order LTI system

$$y(k+2) = \alpha_1 y(k+1) + \alpha_2 y(k) + \beta_0 u(k+1). \tag{2.35}$$

Let the controller have the following structure

$$u(k) = y_r(k+1)/\hat{\beta}_0 - [l_1\hat{\alpha}_1 y(k) + l_2\hat{\alpha}_2 y(k-1)]/\hat{\beta}_0, \tag{2.36}$$

whose parameters are chosen from set N_2, that is, $\hat{\alpha}_1 \in [1.9844, 2.2663]$, $\hat{\alpha}_2 \in [-1.2840, -1]$, $\hat{\beta}_0 \in [0.00075, 0.047]$ and $0 < l_1 \leq 1$, $0 < l_2 \leq 1$.

By following similar steps as in Section (2.2.1), the following conditions are derived under which the closed-loop system is stable:

$$l_2 < 1.7512 l_1, \tag{2.37}$$

$$l_2 < 1.5516 - 1.765 l_1, \tag{2.38}$$

$$0.568 < l_2 < 0.7788. \tag{2.39}$$

We can formulate a similar graph as Fig. 2.1, as shown in Fig. 2.2, in which point P_3 satisfying the golden-section ratio with $l_1 = 0.382$ and $l_2 = 0.618$ lies in the stable region indicated by the shaded triangular area.

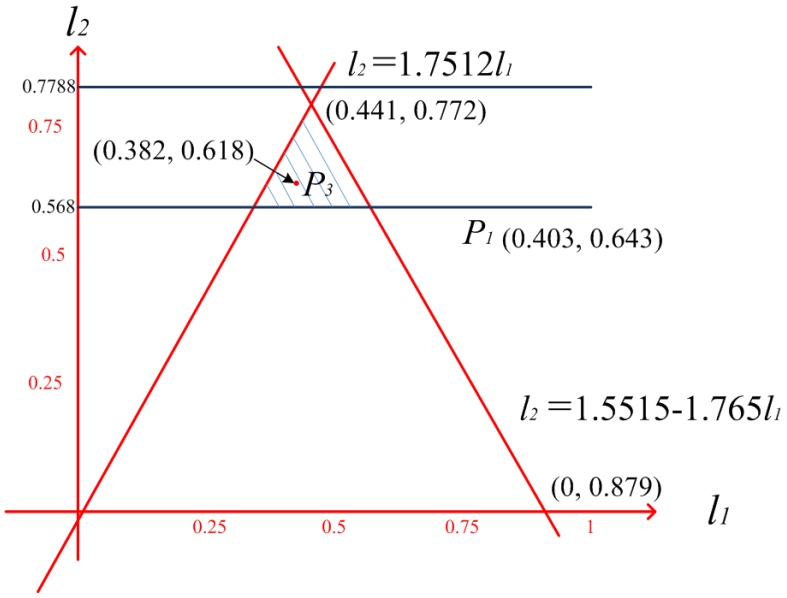

Figure 2.2: Parameter graph for an unstable second order system.

The parameters of an unstable second order system are also given by $\alpha_1 = e^{-T/T_{\min}} + e^{-T/T_{\max}}$, $\alpha_2 = -e^{-T/T_{\min}-T/T_{\max}}$. When $\hat{\alpha}_1 = \alpha_1$, $\hat{\alpha}_2 = \alpha_2$ and $\hat{\beta}_0 = \beta_0$, the characteristic equation of the closed-loop system becomes the same as Eq. (2.28). When $l_1 = 0.382$ and $l_2 = 0.618$,

$$z_{c1} = 0.618e^{-T/T_{\min}}, \tag{2.40}$$

$$z_{c2} = 0.618e^{-T/T_{\max}}. \tag{2.41}$$

While $\frac{T}{T_{\min}} \in [\frac{1}{10}, \frac{1}{4}]$, we can derive

$$|z_{ci}| \leq 0.618e^{0.1} < 0.683, \quad i = 1, 2. \tag{2.42}$$

2.3 Golden-section Adaptive Control

The golden-section robust control method is first analyzed by assuming the controller parameters to be equal to unknown system parameters and the closed-loop stability is achieved. In this section, we will introduce the adaptation algorithm into the golden-section control design and the closed-loop

stability could be achieved even when the estimated parameters do not converge to the true values.

First, Eq. (2.35) is parameterized in the following form:

$$y(k) = \phi^T(k)\theta_p, \tag{2.43}$$

where $\phi(k)$ and $\theta(k)$ are defined as

$$\begin{aligned}\phi(k) &= [y(k-1) \quad y(k-2) \quad u(k-1)]^T,\\ \theta_p &= [\alpha_1 \quad \alpha_2 \quad \beta_0]^T,\end{aligned}$$

$\hat{\theta}(k)$ is the estimate of the parameter vector θ_p and the estimation error $\epsilon(k)$ is given by

$$\epsilon(k) = (\theta_p - \hat{\theta}(k))^T\phi(k) = y(k) - \phi^T(k)\hat{\theta}(k).$$

We adopt the gradient adaptive law and a direct mapping approach to acquire $\hat{\theta}(k)$,

$$\begin{aligned}\hat{\theta}_u(k+1) &= \hat{\theta}(k) + \frac{\gamma\phi(k)\epsilon(k)}{\delta + \phi^T(k)\phi(k)},\\ \hat{\theta}(k+1) &= \pi[\hat{\theta}_u(k+1)],\end{aligned}$$

where $\delta \geq 0$, $0 < \gamma < 2$, and $\pi[x]$ is the projection of x into N_1 or N_2 [31].

The controller has the following structure

$$u(k) = y_r(k+1)/\hat{\beta}_0(k) - [l_1\hat{\alpha}_1(k)y(k) + l_2\hat{\alpha}_2(k)y(k-1)]/\hat{\beta}_0(k), \tag{2.44}$$

where $l_1 = 0.382$, $l_2 = 0.618$, $\hat{\beta}_0(k)$, $\hat{\alpha}_1(k)$ and $\hat{\alpha}_2(k)$ are the estimates of β_0, α_1 and α_2.

The direct mapping means if the estimated parameters are not in the data set N_1 or N_2, the parameters $\hat{\alpha}_1(k)$, $\hat{\alpha}_2(k)$ and $\hat{\beta}_0(k)$ will be assigned values that have the shortest distance between the boundary points of set N_1 or N_2 and estimated values, so the identification results will always remain in the set [31].

The closed-loop system consisting of Eqs. (2.43) and (2.44) can be written as

$$y(k) = \frac{\beta_0}{\hat{\beta}_0(k)} y_r(k) + [\alpha_1 - \frac{\beta_0}{\hat{\beta}_0(k)} l_1 \hat{\alpha}_1(k)] y(k-1) + [\alpha_2 - \frac{\beta_0}{\hat{\beta}_0(k)} l_2 \hat{\alpha}_2(k)] y(k-2). \tag{2.45}$$

If we assume $y_r(k) = 0$ and let $g_1(k) = \alpha_1 - \frac{\beta_0}{\hat{\beta}_0(k)} l_1 \hat{\alpha}_1(k)$ and $g_2(k) = \alpha_2 - \frac{\beta_0}{\hat{\beta}_0(k)} l_2 \hat{\alpha}_2(k)$, we can write the equation into a state space form,

$$\begin{aligned} x(k+1) &= A(k)x(k) + B(k)u(k), \\ y(k) &= C(k)x(k), \end{aligned} \tag{2.46}$$

where

$$A(k) = \begin{bmatrix} 0 & 1 \\ -g_2(k+1) & -g_1(k+1) \end{bmatrix}, \quad B(k) = \begin{bmatrix} 0 \\ 0 \end{bmatrix}, \quad C(k) = \begin{bmatrix} 1 & 0 \end{bmatrix}, \quad x(k) = \begin{bmatrix} y(k) \\ y(k+1) \end{bmatrix}.$$

Although the plant itself is time-invariant, when it is coupled with the adaptive controller, it becomes time-varying. The stability of the closed-loop system 2.45 has been established in [27].

2.4 Simulation Studies

Given a second order system,

$$G_g(z) = \frac{\beta_0 z}{z^2 - \alpha_1 z - \alpha_2}. \tag{2.47}$$

We will consider two different sets of plant coefficients: $\beta_0 = 0.05$, $\alpha_1 = 1.96$, $\alpha_2 = -1.06$ and $\beta_0 = 0.05$, $\alpha_1 = 2.26$, $\alpha_2 = -1.18$. For both sets of coefficients, the plant is unstable.

Compared with the general form indirect adaptive controller ($l_1 = 1$ and $l_2 = 1$), the golden-section adaptive controller does not show advantages in tracking reference input. However, it can provide better performance in terms of stabilization and disturbance rejections, which is extremely important in AMB control applications. The following simulations will demonstrate the capability of golden-section adaptive controller in scenarios of rejecting external disturbance.

In the first set of plant coefficients ($\beta_0 = 0.05$, $\alpha_1 = 1.96$, $\alpha_2 = -1.06$), let the initial conditions be chosen as $\hat{\beta}_0(0) = 0.06$, $\hat{\alpha}_1(0) = 1.92$, $\hat{\alpha}_2(0) = -0.98$. A sinusoidal signal with magnitude of 0.1 and frequency at 30 Hz is considered as the external disturbance. As shown in Fig. 2.3(a), the golden-section adaptive control is able to effectively mitigate the disturbance and keep the the output close to zero and all the estimated coefficients remain bounded.

For the second set of plant coefficients ($\beta_0 = 0.05$, $\alpha_1 = 2.26$, $\alpha_2 = -1.18$), the initial conditions are chosen as $\hat{\beta}_0(0) = 0.1$, $\hat{\alpha}_1(0) = 2$, $\hat{\alpha}_2(0) = -1$. As shown in Fig. 2.3(b), the golden-section adaptive control is also able to effectively mitigate the disturbance and keep the the output close to zero and all the estimated coefficients remain bounded.

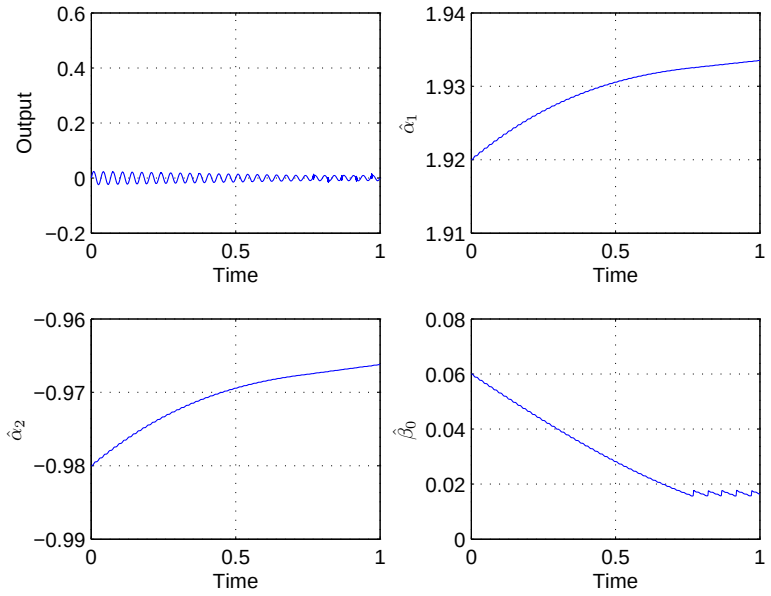

(a) Golden-section adaptive control (1st set of coefficients).

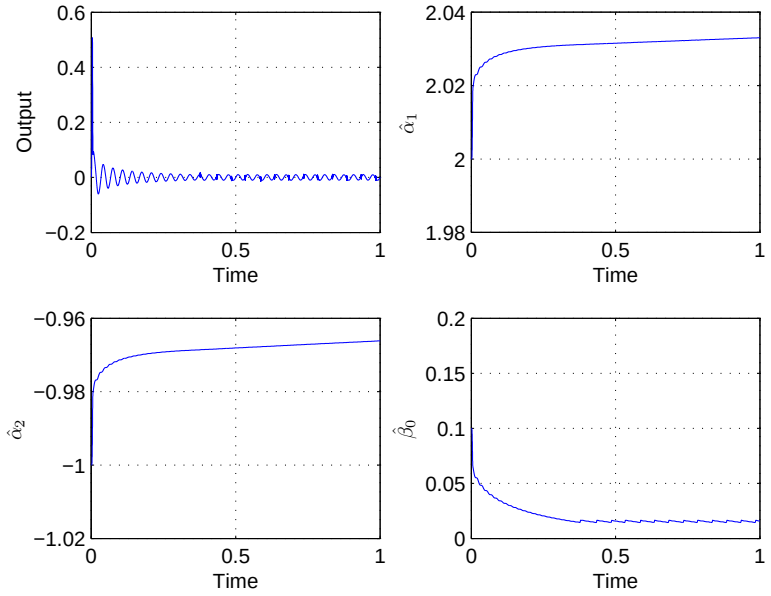

(b) Golden-section adaptive control (2nd set of coefficients).

Figure 2.3: Disturbance rejection and parameter estimates.

Chapter 3

Characteristic Modeling

For systems with simple dynamics, controllers such as PID can sufficiently fulfill the requirements. Therefore, a modeling procedure might not be necessary. For systems with complex structure or even involving nonlinear and time-varying features, although the current modeling method is able to describe the system dynamics and internal information using a mathematical description, the mathematical model might be very complicated. Under this situation, the control design might become difficult. Even though the controller can be designed following the complex model, the controller might have high order, making it difficult to be applied to practical engineering applications. Other modeling approach involves approximating a high order model with a low order model, and the controller design is based on the low order model. This approach reduces the requirement of accurate dynamic analysis but it is not quite feasible for systems with flexible structures [9].

Given the restrictions of conventional modeling methods, one of the most important concerns is the balance between practicality and complexity. With the development of computer technology, the implementation process becomes much easier, which motivates new methods for modeling of complex dynamic systems with high order, time-varying and nonlinearity features. The characteristic modeling method is among one of the options that achieve a good balance. Some preliminary theoretical studies have provided a strong foundation for research and the results have demonstrated its effectiveness and indicated it can significantly simplify controller designs for complex dynamic systems. The characteristic modeling method focuses on the characteristics of the plant and the control performance requirements instead of the precise system dynamics. It compresses the

corresponding information of the high order plant into several characteristic parameters so that no information is lost during the modeling process. Besides, the characteristic model remains a simple structure but it closely represents the dynamics of the original system.

The basic principles of the characteristic modeling can be summarized as follows,

- Given the same input, the output of the characteristic model is the same as the output of the actual plant.
- During the transient process, the output errors remain in a small range that can be ignored.
- The structure and order of the characteristic model is determined by the control requirement, *i.e.*, position tracking or speed tracking.
- Unlike truncated models, characteristic model closely represents the dynamics of a higher order model and it is usually described in a second order slowly time-varying difference equation, where being slowly time-varying means the coefficients of the equation satisfy $\alpha_i(k) \approx \alpha_i(k+1)$.

In this chapter, we will study the characteristic modeling method for the LTI system. Systems will be analyzed and their characteristic models with certain prerequisites will be derived in two cases. Case one focuses on systems with only distinct nonzero real poles. Case two focuses on systems with poles at zero and repeated poles. Several simulation studies will be provided at the end.

3.1 Characteristic Model of LTI Systems

Consider a linear time-invariant plant

$$G(s) = \frac{b_m s^m + b_{m-1} s^{m-1} + \cdots + b_1 s + b_0}{s^n + a_{n-1} s^{n-1} + \cdots + a_1 s + a_0}, \tag{3.1}$$

which can be decomposed as

$$G(s) = \sum_{i=1}^{v} \frac{k_{vi}}{s^i} + \sum_{i=1}^{m} \frac{k_i}{s + \lambda_i} + \sum_{i=1}^{w} \frac{k_{\omega i}}{(s + \lambda_{\omega i})^2}, \tag{3.2}$$

where k_{vi} is a constant gain for the zero pole, k_i is a constant gain for a nonzero real pole $-\lambda_i$, $k_{\omega i}$ are constant gains for repeated real poles $-\lambda_{\omega i}$.

According to the characteristic modeling method [8], if a plant $G(s)$ is given and the control objective is position keeping or tracking, for a sufficiently small sampling period T that satisfies the sampling theorem and guarantees the controllability requirement for the discretized system, its characteristic model is a second-order time-varying difference equation,

$$y(k) = f_1(k)y(k-1) + f_2(k)y(k-2) + g_0(k)u(k-1) + g_1(k)u(k-2), \tag{3.3}$$

where $u(k)$ and $y(k)$ are respectively the control input and the system output at the kth sampling point, $f_1(k)$, $f_2(k)$, $g_0(k)$ and $g_1(k)$ are the characteristic parameters.

If $G(s)$ is stable, its characteristic model possesses the following properties:

- Coefficients $f_1(k)$, $f_2(k)$, $g_0(k)$ and $g_1(k)$ are slowly time-varying.
- The ranges of these parameters can be decided *a priori*.
- In response to the same input, the outputs of the original model and the characteristic model are identical at the sampling points.
- Assume that there are no poles at zero or repeated poles, if the static gain of the system is

  $$D = G(0) = \frac{b_0}{a_0} = 1,$$

  then the sum of all the coefficients approaches 1 in the steady state, *i.e.*,

  $$f_1(\infty) + f_2(\infty) + g_0(\infty) + g_1(\infty) = 1.$$

- If there are poles at zero,

  $$f_1(\infty) + f_2(\infty) = 1.$$

3.2 Characteristic Model of Systems with Distinct Nonzero Poles

First we consider the system with only distinct nonzero poles. For distinct real poles, their output terms y_i have different signs, which is either $y_i > 0$ or $y_i < 0$. If we assume there are l distinct poles that have their output terms $y_i > 0$, $i = 1, \dots l$, and there are $m - l$ distinct poles that have their output terms $y_i < 0$, $i = l + 1, \dots m$, we can assign two groups for the output y_i, $i = 1, \dots m$ as follows,

$$\begin{cases} \frac{dy_1}{dt} + \lambda_1 y_1 = k_1 u(t), \\ \frac{dy_2}{dt} + \lambda_2 y_2 = k_2 u(t), \\ \quad \vdots \\ \frac{dy_l}{dt} + \lambda_l y_l = k_l u(t); \end{cases} \qquad \begin{cases} \frac{dy_{l+1}}{dt} + \lambda_{l+1} y_{l+1} = k_{l+1} u(t), \\ \frac{dy_{l+2}}{dt} + \lambda_{l+2} y_{l+2} = k_{l+2} u(t), \\ \quad \vdots \\ \frac{dy_m}{dt} + \lambda_m y_m = k_m u(t); \end{cases}$$

If we add both sides of the equations separately in the two columns above and rearrange them into two groups based on $y_i > 0$ and $y_i < 0$, the following equations can be obtained,

$$\frac{dy_p}{dt} + a_p y_p = k_p u(t), \tag{3.4}$$

$$\frac{dy_n}{dt} + a_n y_n = k_n u(t), \tag{3.5}$$

where

$$\begin{aligned} y_p &= y_1 + y_2 + \cdots + y_l, \\ k_p &= k_1 + k_2 + \cdots + k_l, \\ a_p &= \frac{\lambda_1 y_1 + \lambda_2 y_2 + \cdots + \lambda_l y_l}{y_p}, \\ y_n &= y_{l+1} + y_{l+2} + \cdots + y_m, \\ k_n &= k_{l+1} + k_{l+2} + \cdots + k_m, \\ a_n &= \frac{\lambda_{l+1} y_{l+1} + \lambda_{l+2} y_{l+2} + \cdots + \lambda_m y_m}{y_n}. \end{aligned}$$

Then we can transform Eqs. (3.4) and (3.5) into difference equations with the Euler discretization method,

$$\frac{y_p(k+1)-y_p(k)}{T}+a_p y_p(k)=k_p u(k)\Rightarrow y_p(k+1)=(1-Ta_p)y_p(k)+Tk_p u(k), \tag{3.6}$$

$$\frac{y_n(k+1)-y_n(k)}{T}+a_n y_n(k)=k_n u(k)\Rightarrow y_n(k+1)=(1-Ta_n)y_n(k)+Tk_n u(k). \tag{3.7}$$

According to engineering experience and the sampling theorem [9], the sampling time T is selected so that

$$T\cdot\max(\lambda_{1\,\max},\lambda_{2\,\max})\leq\frac{1}{15},$$

where

$$0<\lambda_{1\,\min}\leq a_p\leq\lambda_{1\,\max},$$

$$0<\lambda_{2\,\min}\leq a_n\leq\lambda_{2\,\max}.$$

In Eqs. (3.6) and (3.7), $Ta_p<0.1$ and $Ta_n<0.1$. T is usually chosen as $\frac{1}{10}$, so we can further write the equations into the following forms

$$y_p(k+1)=\alpha_p(k)y_p(k)+\beta_p(k)u(k), \tag{3.8}$$

$$y_n(k+1)=\alpha_n(k)y_n(k)+\beta_n(k)u(k), \tag{3.9}$$

where $\alpha_p(k)=1-Ta_p$, $\beta_p(k)=Tk_p$, $\alpha_n(k)=1-Ta_n$ and $\beta_n(k)=Tk_n$.

Because $Ta_p<0.1$ and $Ta_n<0.1$, the changes of a_p and a_n are very small, which implies that the changes of $\alpha_p(k)$ and $\alpha_n(k)$ are very small for every step. We can approximate that $\alpha_p(k)\approx\alpha_p(k+1)$ and $\alpha_n(k)\approx\alpha_n(k+1)$ based on the simulation studies [9]. Because $\beta_p(k)$ and $\beta_n(k)$ only rely on T, it can be observed that $\beta_p(k)=\beta_p(k+1)$ and $\beta_n(k)=\beta_n(k+1)$.

In order to maintain the observability after the discretization, one of the sufficient conditions is that for all the poles that satisfy

$$\mathrm{Re}(\lambda_i-\lambda_j)=0,\quad i,j=1,2,\ldots,h, \tag{3.10}$$

the T needs to satisfy [32]

$$T \neq \frac{2l\pi}{\mathrm{Im}(\lambda_i - \lambda_j)}, \quad l = 1, 2, \dots . \tag{3.11}$$

From the analysis above, we add both sides of Eqs. (3.8) and (3.9) and shift the combined equation one step forward to obtain

$$y_p(k+2) + y_n(k+2) = \alpha_p(k)y_p(k+1) + \alpha_n(k)y_n(k+1) + [\beta_p(k) + \beta_n(k)]u(k+1). \tag{3.12}$$

If we multiple Eq. (3.8) with $\alpha_n(k)$ and Eq. (3.9) with $\alpha_p(k)$ on both sides, the following equations can be obtained

$$\alpha_n(k)y_p(k+1) = \alpha_n(k)\alpha_p(k)y_p(k) + \alpha_n(k)\beta_p(k)u(k), \tag{3.13}$$

$$\alpha_p(k)y_n(k+1) = \alpha_p(k)\alpha_n(k)y_n(k) + \alpha_p(k)\beta_n(k)u(k). \tag{3.14}$$

If we combine Eqs. (3.12), (3.13) and (3.14), let $\tilde{y}(k+i) = y_p(k+i) + y_n(k+i)$, and reorganize all the components, we can obtain the following equation

$$\begin{aligned}\tilde{y}(k+2) = {} & [\alpha_p(k) + \alpha_n(k)]\tilde{y}(k+1) - \alpha_p(k)\alpha_n(k)\tilde{y}(k) + [\beta_p(k) + \beta_n(k)]u(k+1) \\ & - [\alpha_p(k)\beta_n(k) + \alpha_n(k)\beta_p(k)]u(k).\end{aligned} \tag{3.15}$$

Based on the equation above, a second order time-varying difference equation can be described as follows,

$$\tilde{y}(k+2) = \tilde{f}_1(k)\tilde{y}(k+1) + \tilde{f}_2(k)\tilde{y}(k) + \tilde{g}_0(k)u(k+1) + \tilde{g}_1(k)u(k), \tag{3.16}$$

where

$$\begin{aligned}\tilde{f}_1(k) &= \alpha_p(k) + \alpha_n(k) = 2 - T(a_p + a_n), \\ \tilde{f}_2(k) &= -\alpha_p(k)\alpha_n(k) = T(a_p + a_n) - 1 - T^2 a_p a_n, \\ \tilde{g}_0(k) &= \beta_p(k) + \beta_n(k) = T(k_p + k_n), \\ \tilde{g}_1(k) &= -[\alpha_p(k)\beta_n(k) + \alpha_n(k)\beta_p(k)] = T^2(a_p k_n + a_n k_p) - T(k_n + k_p).\end{aligned}$$

3.3 Characteristic Model of Systems with Repeated Poles

Now zero or repeated poles are also considered besides distinct nonzero poles. For simplicity while not losing the generality for the expression, consider the case of $v = 2$. In this case, the outputs resulting from the integral terms can be expressed as

$$\frac{Y_{v1}(s)}{U(s)} = \frac{k_{v1}}{s} \Rightarrow \frac{dy_{v1}(t)}{dt} = k_{v1}u(t), \tag{3.17}$$

$$\frac{Y_{v2}(s)}{U(s)} = \frac{k_{v2}}{s^2} \Rightarrow \frac{d^2y_{v2}(t)}{dt^2} = k_{v2}u(t), \tag{3.18}$$

Eqs. (3.17) and (3.18) can be discretized with the Euler method as,

$$\frac{y_{v1}(k+1) - y_{v1}(k)}{T} = k_{v1}u(k) \Rightarrow y_{v1}(k+1) = y_{v1}(k) + Tk_{v1}u(k), \tag{3.19}$$

and

$$\frac{y_{v2}(k+2) - 2y_{v2}(k+1) + y_{v2}(k)}{T^2} = k_{v2}u(k) \Rightarrow y_{v2}(k+2) = 2y_{v2}(k+1) - y_{v2}(k) + T^2k_{v2}u(k). \tag{3.20}$$

If we shift Eq. (3.19) one step forward and combine the shifted equation with (3.19), the following equation can be derived

$$y_{v1}(k+2) = 2y_{v1}(k+1) - y_{v1}(k) + Tk_{v1}u(k+1) - Tk_{v1}u(k). \tag{3.21}$$

Then we combine Eq. (3.21) with (3.20) so an expression in the form of $y_v(k+i) = y_{v1}(k+i) + y_{v2}(k+i)$ for the zero poles can be obtained

$$y_v(k+2) = 2y_v(k+1) - y_v(k) + Tk_{v1}u(k+1) + (T^2k_{v2} - Tk_{v1})u(k). \tag{3.22}$$

For repeated poles, if we pick $w = 1$ without loss of generality, the output terms of the repeated poles can be expressed as

$$\frac{Y_{\omega1}(s)}{U(s)} = \frac{k_{\omega1}}{(s+\lambda_{\omega1})^2} \Rightarrow \frac{d^2y_{\omega1}(t)}{dt^2} + 2\lambda_{\omega1}\frac{dy_{\omega1}(t)}{dt} + \lambda_{\omega1}^2 y_{\omega1}(t) = k_{\omega1}u(t), \tag{3.23}$$

and the discretized form of Eq. (3.23) can be described as follows,

$$y_{\omega 1}(k+2) = (2 - 2T\lambda_{\omega 1})y_{\omega 1}(k+1) + (T^2\lambda_{\omega 1}^2 - 1 + 2T\lambda_{\omega 1})y_{\omega 1}(k) + T^2 k_{\omega 1}u(k). \tag{3.24}$$

According to engineering experience and the sampling theorem, the sampling time T is selected so that [9]

$$T \cdot \max(\lambda_{1\,\max}, \lambda_{2\,\max}, \lambda_{\omega 1}) \leq \frac{1}{200}.$$

So $T \leq 0.005$ and $T^2 \to 0$, we can approximate $T^2\lambda_{\omega 1}^2 - 1 + 2T\lambda_{\omega 1}$ with $2T\lambda_{\omega 1} - 1$.

Once we combine Eq. (3.22) with Eq. (3.24) and rearrange the new equation in the form of $\bar{y}(k+i) = y_v(k+i) + y_{\omega 1}(k+i)$, the following equation can be obtained

$$\begin{aligned}\bar{y}(k+2) = {} & 2(1 - T\lambda_{\omega 1})\bar{y}(k+1) + (2T\lambda_{\omega 1} - 1)\bar{y}(k) + Tk_{v1}u(k+1) + (T^2k_{v2} - Tk_{v1} + T^2k_{\omega 1})u(k) \\ & + 2T\lambda_{\omega 1}(y_v(k+1) - y_v(k)).\end{aligned}$$

The term $2T\lambda_{\omega 1}(y_v(k+1) - y_v(k))$ represents the modeling error. Since $2T\lambda_{\omega 1} \leq 0.02$ and $y_v(k+1) - y_v(k) \approx 0$ in the steady state, $2T\lambda_{\omega 1}(y_v(k+1) - y_v(k))$ can be ignored. The simplified equation can be written as follows,

$$\bar{y}(k+2) = 2(1 - T\lambda_{\omega 1})\bar{y}(k+1) + (2T\lambda_{\omega 1} - 1)\bar{y}(k) + Tk_{v1}u(k+1) + (T^2k_{v2} - Tk_{v1} + T^2k_{\omega 1})u(k). \tag{3.25}$$

By combining Eq. (3.16) with Eq. (3.25) in the form of $y(k+i) = \tilde{y}(k+i) + \bar{y}(k+i)$, the following result can be obtained,

$$\begin{aligned}y(k+2) = {} & [\alpha_p(k) + \alpha_n(k)]y(k+1) - \alpha_p(k)\alpha_n(k)y(k) + [\beta_p(k) + \beta_n(k) + Tk_{v1}]u(k+1) \\ & - [\alpha_p(k)\beta_n(k) + \alpha_n(k)\beta_p(k) - (T^2k_{v2} - Tk_{v1} + T^2k_{\omega 1})]u(k) \\ & + \epsilon_1(k)\bar{y}(k+1) - \epsilon_2(k)\bar{y}(k),\end{aligned} \tag{3.26}$$

where

$$\epsilon_1(k) = 2(1 - T\lambda_{\omega 1}) - [\alpha_p(k) + \alpha_n(k)] = T(a_p + a_n - 2\lambda_{\omega 1}),$$
$$\epsilon_2(k) = (1 - 2T\lambda_{\omega 1}) + \alpha_p(k)\alpha_n(k) = T(a_p + a_n - 2\lambda_{\omega 1}) - T^2 a_p a_n.$$

Since $2T\lambda_{\omega 1} \leq 0.01$, $T^2 a_p a_n \leq 0.0001$, the difference between $\epsilon_1(k)$ and $\epsilon_2(k)$ is determined by $-T^2 a_p a_n$, which is quite small that can be ignored, so $\epsilon_1(k) \approx \epsilon_2(k)$. Besides, $\bar{y}(k+1) - \bar{y}(k) \approx 0$ in the steady state, so this modeling error $\epsilon_1(k)\bar{y}(k+1) - \epsilon_2(k)\bar{y}(k)$ can be ignored for the analysis. Therefore, the final second order time-varying difference equation can be written as

$$y(k+2) = f_1(k)y(k+1) + f_2(k)y(k) + g_0(k)u(k+1) + g_1(k)u(k), \tag{3.27}$$

where

$$f_1(k) = \alpha_p(k) + \alpha_n(k) = 2 - T(a_p + a_n),$$
$$f_2(k) = -\alpha_p(k)\alpha_n(k) = T(a_p + a_n) - 1 - T^2 a_p a_n,$$
$$g_0(k) = \beta_p(k) + \beta_n(k) + Tk_{v1} = T(k_p + k_n + k_{v1}),$$
$$g_1(k) = T^2(k_{v2} + k_{\omega 1}) - Tk_{v1} - \alpha_p(k)\beta_n(k) - \alpha_n(k)\beta_p(k)$$
$$= T^2(k_{v2} + k_{\omega 1} + a_p k_n + a_n k_p) - T(k_{v1} + k_n + k_p).$$

3.4 Simulation Studies

In this section, several simulation examples will be provided to illustrate how to acquire the characteristic model from the original system. We will use a least-squares adaptive estimation algorithm for the parameter estimates. The parameter estimation is important for the adaptive control system design because all the characteristic parameter estimates will be directly used in the controller. A standard characteristic model is given as follows,

$$y(k) = f_1(k)y(k-1) + f_2(k)y(k-2) + g_0(k)u(k-1) + g_1(k)u(k-2),$$

and it can be parameterized as

$$y(k) = \theta^T(k)\phi(k), \tag{3.28}$$

where

$$\theta(k) = [f_1(k) \quad f_2(k) \quad g_0(k) \quad g_1(k)]^T, \tag{3.29}$$

$$\phi(k) = [y(k-1) \quad y(k-2) \quad u(k-1) \quad u(k-2)]^T. \tag{3.30}$$

The least-squares algorithm is described as below

$$\begin{aligned} N(k) &= \frac{P(k-1)\phi(k-1)}{\lambda + \phi^T(k-1)P(k-1)\phi(k-1)}, \\ P(k) &= \frac{1}{\lambda}[I - N(k)\phi^T(k)]P(k-1), \\ \hat{\theta}(k) &= \hat{\theta}(k-1) + N(k)[y(k) - \phi^T(k-1)\hat{\theta}(k-1)], \end{aligned}$$

where $\hat{\theta}(k)$ are estimates of the parameter vector $\theta(k)$ and λ is the forgetting factor.

The estimation error is defined as

$$\epsilon(k) = y(k) - \phi^T(k-1)\hat{\theta}(k-1).$$

The least-squares parameter estimation algorithm guarantees the following properties [30]:

- $P(k) = P^T(k) > 0, \forall k \in k_0, k_0+1, \ldots$, and $P(k)$ is bounded;
- $\theta(k)$ and $\frac{\epsilon(k)}{\bar{m}(k)}$ are bounded, where $\bar{m}(k) = \sqrt{\lambda + \phi^T(k-1)\phi(k-1)}$;
- $\frac{\epsilon(k)}{m(k)}$ belongs to L^2, where the signal space $L^2 = \{x(t) \in R^n : \|x(\cdot)\|_2 < \infty\}$, $m(k) = \sqrt{\phi^T(k-1)P(k-1)\phi(k-1)}$; $\frac{\epsilon(k)}{\bar{m}(k)}$ and $\theta(k) - \theta(k-1)$ belong to L^2;
- There exist a constant matrix P_∞ and a constant vector θ_∞ such that $\lim_{k\to\infty} P(k) = P_\infty$ and $\lim_{k\to\infty} \theta(k) = \theta_\infty$.

The following reference input signals are used to compare the output of the original plant and its characteristic model with a sampling time $T = 0.001s$:

1. A step input $r_1(k) = 10\mathrm{u}(k)$;

2. Sinusoidal input $r_2(k) = 10\sin(0.05\pi kT) + 5\sin(2.5\pi kT) + 0.8\sin(60\pi kT)$;

3. Random input $r_3(k) = 10\mathrm{u}(k-15) + 5\mathrm{u}(k-5) + 10\mathrm{u}(k) + 10\sin(0.05\pi kT) + \mathrm{sgn}(\sin(0.4\pi kT))$.

3.4.1 Characteristic modeling of systems with distinct nonzero poles

The first plant $G_1(s)$ includes only distinct nonzero poles

$$G_1(s) = \frac{s^3 + 11.5s^2 + 29.5s + 12}{s^6 + 29s^5 + 1531s^4 + 12479s^3 + 35150s^2 + 45450s + 26500},$$

which has three zeros $z_1 = -0.5$, $z_2 = -3$, $z_3 = -8$, and six poles $p_1 = -2$, $p_2 = -5$, $p_3 = -1 + 1j$, $p_4 = -1 - 1j$, $p_5 = -10 + 35j$, $p_6 = -10 - 35j$, and is a stable minimum phase system.

Its discrete-time transfer function can be described as follows,

$$G_1(z) = \frac{Y(z)}{U(z)} = \frac{10^{-10}(1.659z^5 + 1.649z^4 - 13.17z^3 + 13.12z^2 - 1.637z - 1.627)}{z^6 - 5.97z^5 + 14.85z^4 - 19.71z^3 + 14.71z^2 - 5.856z + 0.9714},$$

and its corresponding difference equation is given by

$$\begin{aligned} y(k) = {} & 5.97y(k-1) - 14.85y(k-2) + 19.71y(k-3) - 14.71y(k-4) + 5.856y(k-5) - 0.9714y(k-6) \\ & + 10^{-10}(1.659u(k-1) + 1.649u(k-2) - 13.17u(k-3) + 13.12u(k-4) - 1.637u(k-5) - 1.627u(k-6)). \end{aligned}$$

Based on the least-squares parameter estimation algorithm, we can perform the parameter estimation and the initial values of the characteristic parameters need to satisfy the following requirements:

- Given there are no zero poles, $f_1(k_0) + f_2(k_0) + g_0(k_0) + g_1(k_0) = 1$;
- The selection of all characteristic parameters should make the system stable, which can be verified using the Jury test;
- According to the all-coefficient adaptive control method presented in Chapter 2, $f_1(k_0)$ should be close to 2 and $f_2(k_0)$ should be negative but bigger than -1, both $g_0(k_0)$ and $g_1(k_0)$ should be much smaller than 1.

Therefore, the following set of initial values are selected:

$$f_1(k_0) = 1.996, \quad f_2(k_0) = -0.999, \quad g_0(k_0) = 1.7 * 10^{-7}, \quad g_1(k_0) = 1.3 * 10^{-7}$$

for its characteristic model

$$y_1(k) = f_1(k)y_1(k-1) + f_2(k)y_1(k-2) + g_0(k)u(k-1) + g_1(k)u(k-2).$$

By using three different reference inputs, the comparison between G_1 and its characteristic model GC_1 are shown as follows,

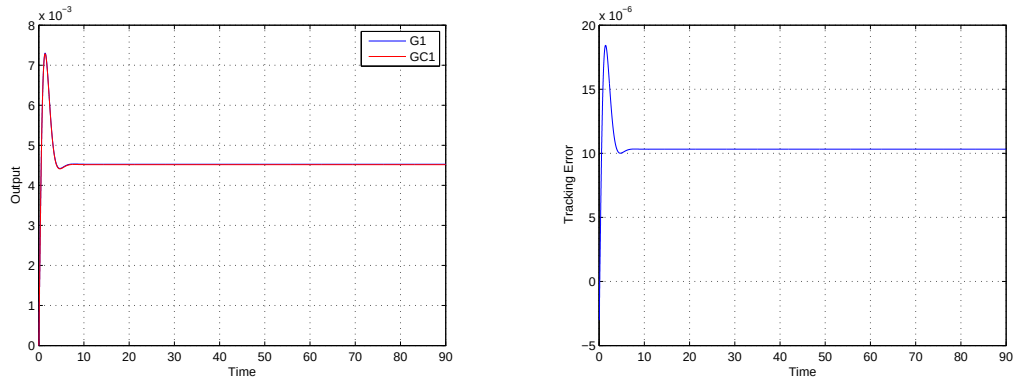

(a) Output comparison. (b) Modeling error.

Figure 3.1: Model comparison with a step input signal.

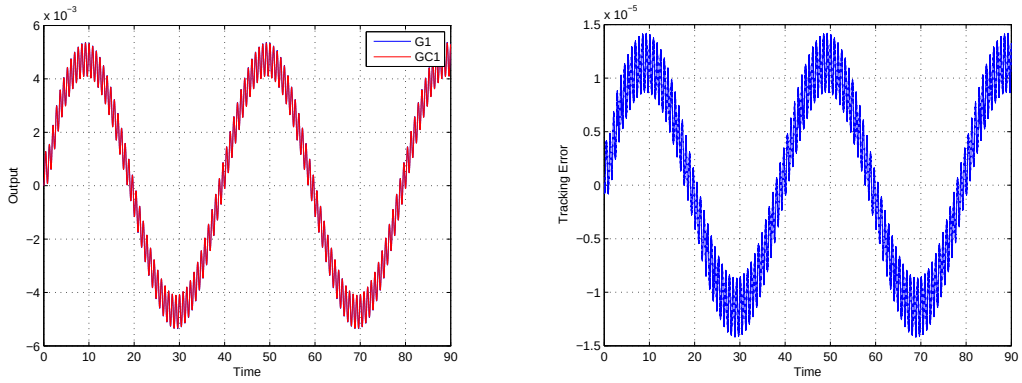

(a) Output comparison. (b) Modeling error.

Figure 3.2: Model comparison with sinusoidal input signals.

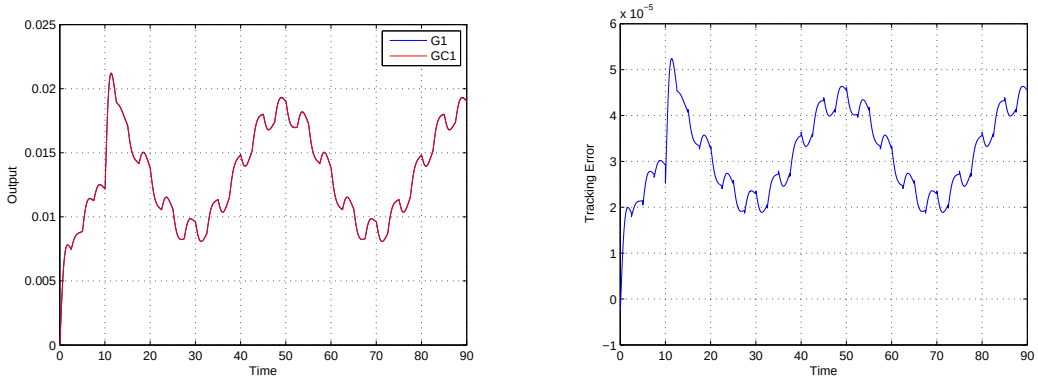

(a) Output comparison. (b) Modeling error.

Figure 3.3: Model comparison with random input signals.

As shown in Fig. 3.1, a unit step signal is used as the referenced input. The characteristic model is able to track the transient response and steady state response of the original plant and maintain a small modeling error under 2×10^{-5}. In Fig. 3.2, the sinusoidal output of the characteristic model is very close to the output of the original plant and the modeling error is below 1.5×10^{-5}. When given a random input as shown in Fig. 3.3, even though there are many different transitions and no steady state, the characteristic can still retain a tracking error under 6×10^{-5}.

3.4.2 Characteristic modeling of systems with repeated poles

The second plant $G_2(s)$ includes zero poles and repeated real poles besides the distinct nonzero poles as in case 1

$$G_2(s) = \frac{s^3 + 11.5s^2 + 29.5s + 12}{s^8 + 34s^7 + 1676s^6 + 20134s^5 + 97545s^4 + 221200s^3 + 253750s^2 + 132500s},$$

which contains three zeros $z_1 = -0.5$, $z_2 = -3$, $z_3 = -8$, and eight poles $p_1 = 0$, $p_2 = -2$, $p_3 = -1 + 1j$, $p_4 = -1 - 1j$, $p_5 = -10 + 35j$, $p_6 = -10 - 35j$, $p_7 = p_8 = -5$ so it has one integral component and one repeated pole.

Its discrete-time transfer function can be described as follows,

$$G_2(z) = \frac{Y(z)}{U(z)} = \frac{10^{-17}(0.83z^7 + 19.03z^6 - 7.42z^5 - 78z^4 + 77.72z^3 + 7.34z^2 - 18.68z - 0.809)}{z^8 - 7.965z^7 + 27.76z^6 - 55.27z^5 + 68.8z^4 - 54.81z^3 + 27.29z^2 - 7.764z + 0.9665},$$

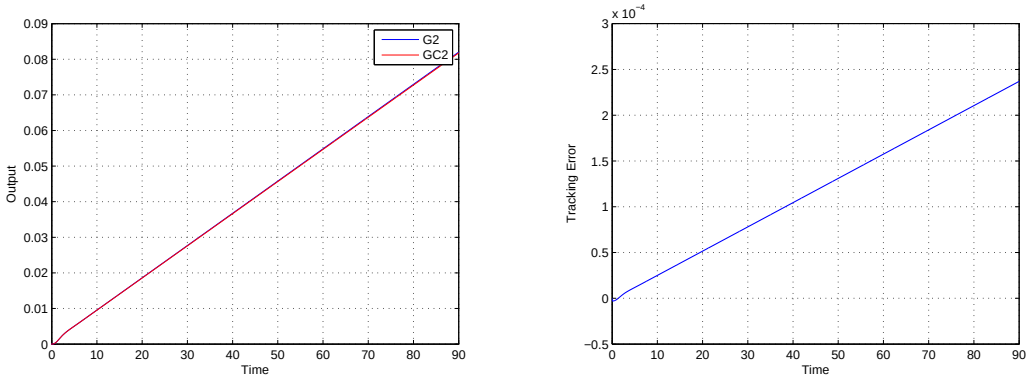

(a) Output comparison. (b) Modeling error.

Figure 3.4: Model comparison with a step input signal.

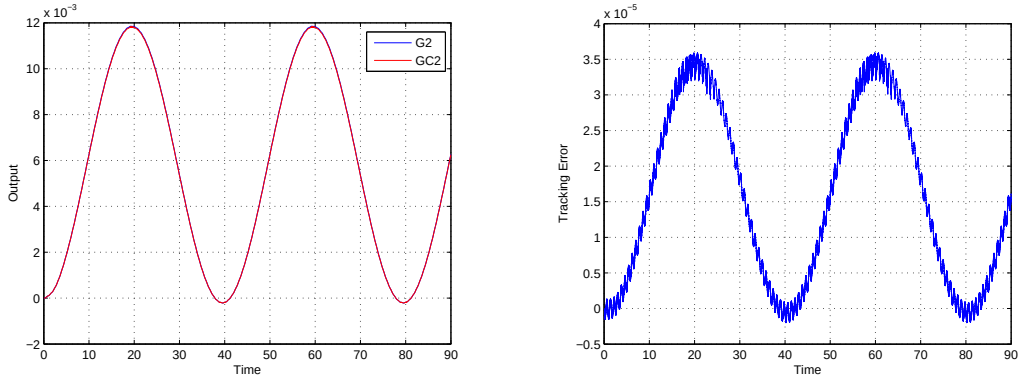

(a) Output comparison. (b) Modeling error.

Figure 3.5: Model comparison with sinusoidal input signals.

and its corresponding difference equation can be obtained,

$$\begin{aligned} y(k) = {} & 7.965y(k-1) - 27.76y(k-2) + 55.27y(k-3) - 68.8y(k-4) + 54.81y(k-5) - 27.29y(k-6) \\ & + 7.764y(k-7) - 0.9665y(k-8) + 10^{-17}[0.83u(k-1) + 19.03u(k-2) - 7.42u(k-3) \\ & - 78u(k-4) + 77.72u(k-5) + 7.34u(k-6) - 18.68u(k-7) - 0.809u(k-8)]. \end{aligned}$$

According to the least-squares parameter estimation algorithm, using different reference inputs, the comparison between G_2 and its characteristic model GC_2 are shown as follows,

As shown in Fig. 3.4, a unit step signal is used as the referenced input. Due to the zero pole, the integral effect causes the system output to keep increasing while the characteristic model is able to

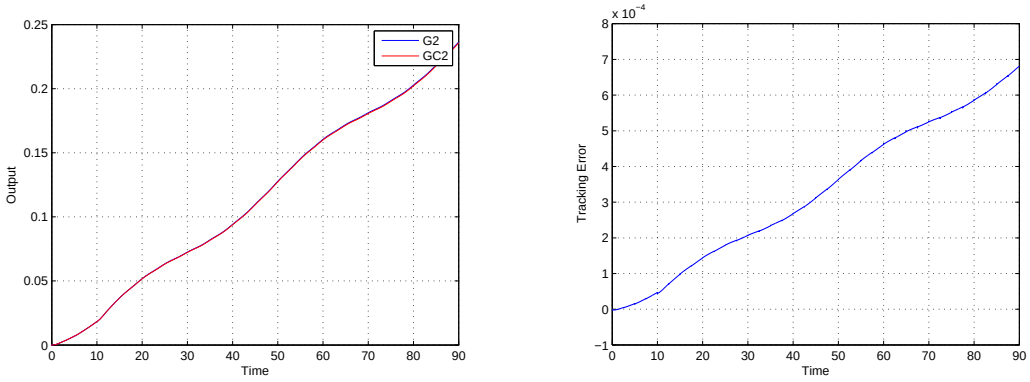

(a) Output comparison. (b) Modeling error.

Figure 3.6: Model comparison with random input signals.

track the response of the original plant. However, with time increasing, the modeling error will get bigger and the model accuracy gets degraded. In Fig. 3.5, the sinusoidal output of the characteristic model is very close to the output of the original plant and the modeling error is below 4×10^{-5}. Given a random input as shown in Fig. 3.6, although the output of the characteristic model can still track the original plant, the tracking error still keeps increasing and the characteristic model will become less accurate.

Chapter 4

Characteristic Model Based ACAC on AMBs

As shown in the previous chapters, the all-coefficient adaptive control method was applied to LTI systems with unknown system parameters and we can achieve desired stabilization and disturbance rejection performance. The characteristic modeling is able to capture the essential dynamics of a high order time-invariant plant by using a second order time-varying difference equation. It provides theoretical foundations for low order controllers to handle high order plants with unknown parameters. Therefore, it is legitimate to consider combining those two methods for application to systems with complex dynamics.

The characteristic model based ACAC method has been studied and applied to several industrial applications [8, 9, 31, 33, 34]. Compared with conventional adaptive control, characteristic model based ACAC has fewer coefficients to estimate and the controller structure is much simpler. It has been shown the output of characteristic model is almost identical to that of the high order LTI model when the sampling time is sufficiently small. The unknown coefficients can be identified using either gradient or least-squares methods, and they are projected into the ranges specified by the all-coefficient adaptive control method. Currently we will focus on the single input single output (SISO) characteristic model and synthesize the maintaining/tracking, linear feedback, logical differental/integral control algorithms so different control design scenarios can be achieved.

In this chapter, we will apply the characteristic model based ACAC method to stabilize a flexible

rotor AMB test rig. First we will briefly describes the test rig and an existing μ-synthesis controller. Then the concept of all-coefficient adaptive control mechanism based on characteristic model will be introduced. Afterwards, we will show the characteristic modeling of the rotor AMB model, present the implementation and show comprehensive simulation and experimental results at the end.

4.1 Test Rig and AMB Control

The AMB test rig [35] was designed and built as a research platform in the Rotating Machinery and Controls (ROMAC) Laboratory at University of Virginia. The original purpose of this test rig is to emulate an industrial centrifugal gas compressor and study control of the rotordynamic instability as shown in Fig. 4.1. Disk 1 and disk 2 on our test rig simulate the wheels in a compressor and the exciter AMB in the middle synthesizes the effect of a seal. When the speed increases, the disks will generate the gyroscopic effect and that can drive the eigenvalues of rotor bending modes away from the original locations. This model uncertainty could cause instabilities issues. The load-dependent cross coupling stiffness (CCS) from the exciter AMB is another important control challenge because the CCS can move the poles in the right half plane (RHP) even deeper to the right and move zeros into the RHP, which also causes instability issues [36].

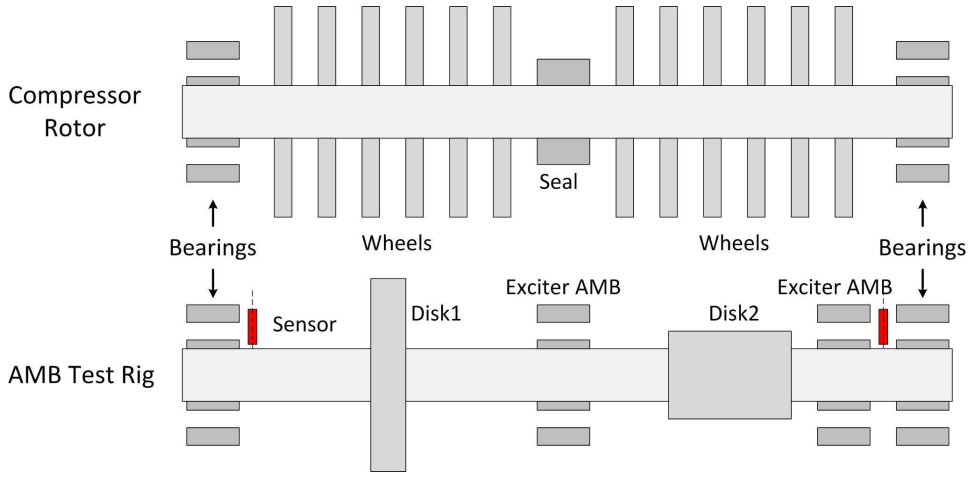

Figure 4.1: Design motivation.

Many experimental challenges have been encountered and solved during the design and construction process. The original displacement sensors were sensitive to the inductive and capacitive coupled noise and we improved the circuit design by adding an anti-aliasing filter and using the

grounding/shielding technique. The sensor runout was also an issue and we improved the outer-diameter (OD) grinding of all sensing planes and rotor laminations to solve the problem. The shaft was originally driven by a timing belt and pulley system and that caused a misalignment issue. We replaced it with a direct-drive transmission and high-speed motor to address the drive-line misalignment. The foundation/substructure mode issues also needed to be addressed because our operating speed would cross those frequencies and we needed to make sure they were within our controller bandwidth. We solved the problem by tuning the sensor mounts and stiffening the bearing pedestals.

The rotor is 1.23 m long and weighs around 44.9 kg. Four laminated steel journals are mounted on the shaft for two radial support AMBs at the nondriven end (NDE) and driven end (DE), and two radial disturbance AMBs at the middle and quarter span, which can be observed in Fig. 4.2. Only the NDE and DE support AMBs are utilized for control. The first rigid body mode is around 2500 RPM (41.67 Hz) and the first bending mode is around 14800 RPM (246.67 Hz). There are also two auxiliary ball bearings mounted at the support AMB locations to prevent damage to AMBs when the rotor drops. A 3.7 kW Colombo RS-90/2, electric fan cooled, high speed motor with variable frequency drive (VFD) is used to make the rotor run up to 18,000 RPM, and a 2.2 Nm motor torque is also available for this speed.

Four amplifiers are installed for each radial magnetic bearing and each amplifier features a 25 kHz switching frequency. The maximum continuous current rates at 10 A, which gives each AMB a static load capacity of 1450 N. The rotor motion is monitored by a 10 channel Kaman eddy current sensor system and the displacement of each control axis is measured by a 1H/15N static probe. The digital control system is based on the Innovative Integration M6713 PCI board and a TI C6713B 32-bit floating point digital signal processing (DSP) chip is used for the implementation of the digital control algorithm with an updating frequency around 12 kHz. There are 16 channels of analog input and output to be simultaneously sampled and interfaced with the actuators and sensors. A control station computer with custom graphic user interface is also designed to provide the user with many functionalities. The entire AMB test rig is shown in Fig. 4.3.

Closed-loop feedback control is critical for the stabilization of an AMB system. The μ-synthesis approach is applied to the AMB control design using Matlab function dksyn for D-K iteration with 4 iterations to find a reasonable μ value [36]. A frequency domain weighting functions and

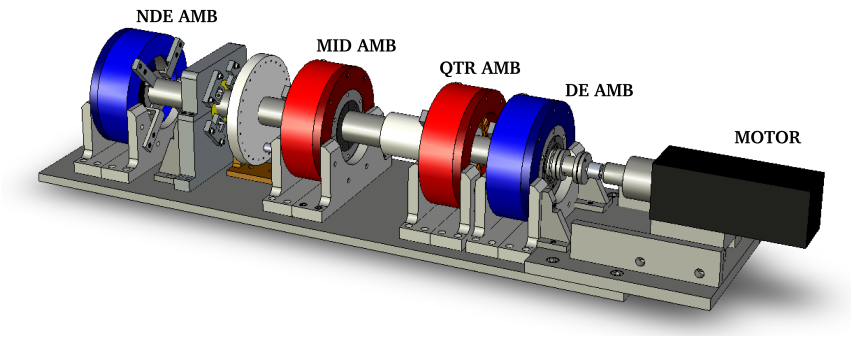

Figure 4.2: Test rig assembly.

mixed-sensitivity optimizations are adopted to define the performance specification. Detailed designs of the μ-synthesis controller can be referred to [36]. The final μ-synthesis design is a 48th order controller with $\mu = 0.856$ for the plant model of 36 states, which include models of the rotor dynamics, AMBs, sensors, amplifiers and other components. In Simulink, it is implemented in a state space form for the x and y axes of both DE and NDE [6]. This design is later implemented in a DSP computer and the performance requirement and parametric uncertainties of the rotor-AMB system have been well handled by the μ-synthesis control [36]. We will use the designed μ controller as a baseline to compare the proposed characteristic model based ACAC method with.

4.2 Characteristic Model Based All-coefficient Adaptive Control

For a linear time-invariant plant that can be described as

$$G(s) = \frac{b_m s^m + b_{m-1} s^{m-1} + \cdots + b_1 s + b_0}{s^n + a_{n-1} s^{n-1} + \cdots + a_1 s + a_0}, \tag{4.1}$$

where $m < n$.

Its characteristic model is given as follows,

$$y(k) = f_1(k)y(k-1) + f_2(k)y(k-2) + g_0(k)u(k-1) + g_1(k)u(k-2). \tag{4.2}$$

where $f_1(k)$, $f_2(k)$, $g_0(k)$ and $g_1(k)$ are the characteristic parameters.

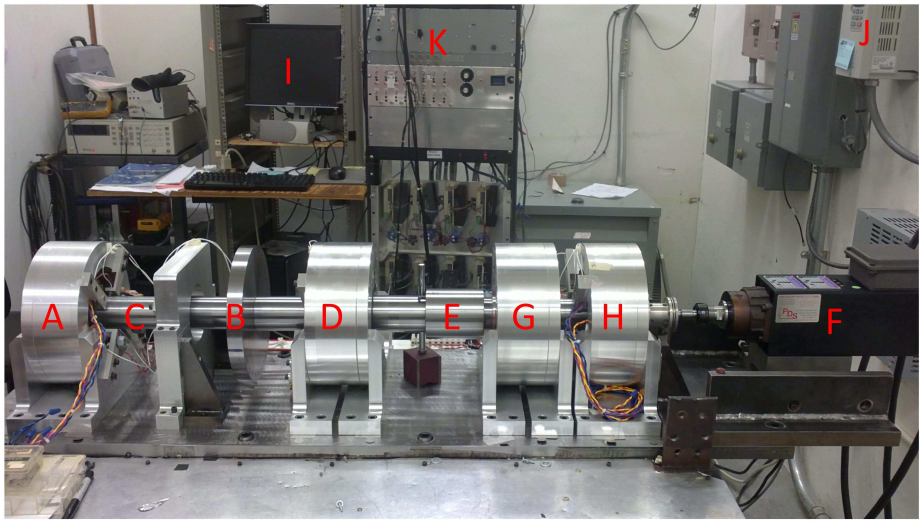

Figure 4.3: Test rig components.

The characteristic model can be parameterized as follows,

$$y(k) = \phi^T(k)\theta(k),$$

where $\phi(k)$ and $\theta(k)$ are defined as

$$\phi(k) = [y(k-1) \quad y(k-2) \quad u(k-1) \quad u(k-2)]^T,$$
$$\theta(k) = [f_1(k) \quad f_2(k) \quad g_0(k) \quad g_1(k)]^T.$$

In order to specify the ranges of the parameters, we first analyze a second order time-invariant difference equation as

$$y(k) = \alpha_1 y(k-1) + \alpha_2 y(k-2) + \beta_0 u(k-1) + \beta_1 u(k-2).$$

It has been shown in Chapter 2 that the parameters follow

$$\begin{aligned}
\alpha_1 &= e^{-T/T_{\min}} + e^{-T/T_{\max}},\\
\alpha_2 &= -e^{-T/T_{\min}-T/T_{\max}},\\
\beta_0 &= k_1 T_{\max}(1 - e^{-T/T_{\max}}) + k_2 T_{\min}(1 - e^{-T/T_{\min}}),\\
\beta_1 &= k_1 T_{\max}(e^{-T/T_{\max}-T/T_{\min}} - e^{-T/T_{\min}}) + k_2 T_{\min}(e^{-T/T_{\max}-T/T_{\min}} - e^{-T/T_{\max}}).
\end{aligned}$$

where $T_{\max} = 1/p_1$ and $T_{\min} = 1/p_2$. p_1 and p_2 are the poles of the transfer function (2.8) and k_1 and k_2 are the constant gains.

Let the ratio between the sampling time and the minimum equivalent time constant $\eta = \frac{T}{T_{\min}}$ satisfy $\eta \in [0, \eta_{\max}]$ and the ratio between the sampling time and the maximum equivalent time constant satisfy $\frac{T}{T_{\max}} \in [0, \frac{T}{T_{\min}}]$. It has been shown the parameters satisfy the following conditions for unstable plants [29]:

$$\begin{cases}
2\cos(\frac{\eta_{\max}}{2}) \leq \alpha_1 \leq 2e^{\frac{\eta_{\max}}{2}},\\
-e^{\eta_{\max}} < \alpha_2 \leq -1,\\
2e^{\frac{\eta_{\max}}{2}}\cos(\frac{\eta_{\max}}{2}) - e^{\eta_{\max}} \leq \alpha_1 + \alpha_2 < -1,\\
\frac{b_0 T^2}{2} < \beta_0 < \frac{b_0 T^2}{2}(1 + \frac{\eta_{\max}}{3} + \frac{\eta_{\max}^2}{12}),\\
\frac{b_0 T^2}{2}(1 - \frac{\eta_{\max}^2}{24}) < \beta_1 < \frac{b_0 T^2}{2}(1 + \frac{2\eta_{\max}}{3} + \frac{7\eta_{\max}^2}{24}).
\end{cases}$$

Based on the conditions above, it can be observed that $\alpha_1 \to 2$, $\alpha_2 \to -1$, $\beta_0 \to 0$, $\beta_1 \to 0$ and $\alpha_1 + \alpha_2 + \beta_0 + \beta_1 \to 1$ as $T \to 0$. Let

$$\begin{cases}
\frac{T}{T_{\min}} \in [\frac{1}{10}, \frac{1}{4}],\\
\frac{T}{T_{\max}} \in [0, \frac{1}{10}].
\end{cases}$$

Then the ranges for the corresponding parameters can be calculated with $\eta_{\max} = \frac{1}{4}$ [24],

$$\begin{cases} \alpha_1 \in [1.9844, 2.2663], \\ \alpha_2 \in [-1.2840, -1], \\ \alpha_1 + \alpha_2 \in [0.9646, 1]. \end{cases}$$

Because β_0 and β_1 are close to 0, we can choose some small positive numbers as initial values for $g_0(k)$ and $g_1(k)$. For the initial values of the other parameter estimates, $f_1(k)$ and $f_2(k)$ are to be chosen from

$$N = \{(f_1(k), f_2(k)) \mid 1.9844 < f_1(k) < 2.2663, -1.2840 < f_2(k) < -1\}.$$

Let $\hat{\theta}(k)$ be the estimate of the time-varying parameter vector $\theta(k)$ and the estimation error $\epsilon(k)$ is

$$\epsilon(k) = y(k) - \phi^T(k)\hat{\theta}(k) = (\theta(k) - \hat{\theta}(k))^T\phi(k).$$

We can adopt the gradient adaptive law and a direct mapping approach to acquire $\hat{\theta}(k)$ as,

$$\begin{aligned} \hat{\theta}_u(k+1) &= \hat{\theta}(k) + \frac{\gamma\phi(k)\epsilon(k)}{\delta + \phi^T(k)\phi(k)}, \\ \hat{\theta}(k+1) &= \pi[\hat{\theta}_u(k+1)], \end{aligned}$$

where $\delta \geq 0$, $0 < \gamma < 2$, and $\pi[x]$ is the projection of x into N [31].

The characteristic model based all-coefficient adaptive control scheme $u_c(k)$ for the AMB control is written as

$$u_c(k) = u_{c1}(k) + u_{c2}(k) + u_{c3}(k) + u_{c4}(k),$$

where $u_{c1}(k)$, $u_{c2}(k)$, $u_{c3}(k)$ and $u_{c4}(k)$ are respectively specified as

1. Maintaining/tracking control

$$u_{c1}(k) = \frac{y_r(k) - \hat{f}_1(k)y(k) - \hat{f}_2(k)y(k-1) - \hat{g}_1(k)u_{c1}(k-1)}{\hat{g}_0(k) + \lambda_1},$$

where $y_r(k)$ is the desired output, λ_1 is a positive constant, and $\hat{g}_0(k)$, $\hat{f}_1(k)$, $\hat{f}_2(k)$ and $\hat{g}_1(k)$ are the estimates of $g_0(k)$, $f_1(k)$, $f_2(k)$ and $g_1(k)$, respectively;

2. Golden-section adaptive control

$$u_{c2}(k) = \frac{l_{c1}\hat{f}_1(k)\tilde{y}(k) + l_{c2}\hat{f}_2(k)\tilde{y}(k-1) + \hat{g}_1(k)u_{c2}(k-1)}{\hat{g}_0(k) + \lambda_1},$$

where $\tilde{y}(k) = y_r(k) - y(k)$, $l_{c1} = 0.382$ and $l_{c2} = 0.618$;

3. Differential control

$$u_{c3}(k) = d_1\frac{\tilde{y}(k) - \tilde{y}(k-1)}{T},$$

where d_1 is a positive constant;

4. Integral control

$$u_{c4}(k) = d_2\sum_{i=1}^{k}\tilde{y}(i) = u_{c4}(k-1) + d_2\tilde{y}(k),$$

where d_2 is a positive constant.

4.3 Characteristic Modeling of the Rotor-AMB System

The original flexible rotor AMB system has very complex dynamics and many components are involved in the modeling process. For the rotor, a two dimensional rotor model is derived from finite-element analysis by dividing the shaft length into 50 stations for the lateral rotordynamic analysis. For the AMB, a linear magnetic circuit model as shown in the introduction was used. For the sensor, anti-aliasing filter (AAF) and amplifier, they are described using transfer functions. A *Páde* approximation is used to approximate the computational delay from DSP. The original model has 452 element state vector. Because the higher modes beyond the third bending mode contribute

negligible effect in the system dynamic response, they are truncated and the final reduced order model possesses 36 element state vector with 4 inputs and 4 outputs for driven end x (DEX) axis, driven end y (DEY) axis, non-driven end x (NDEX) axis and non-driven end y (NDEY) axis.

For the flexible rotor AMB system, its motion equation can be described as follows,

$$M\ddot{z} + (C + G\Omega)\dot{z} + Kz = F_{mag} + F_m + F_{unb} + F_w,$$

where

- M is the mass matrix, C is the damping matrix, G is the gyroscopic matrix and K is the damping matrix, Ω is the rotating speed;
- $z = [x_d \quad y_d \quad x_{nd} \quad y_{nd}]^T$, x_d and y_d are the radial displacements of shaft in the driven end, x_{nd} and y_{nd} are the radial displacements of shaft in the non driven end;
- $F_m = [0 \quad mg \quad 0 \quad mg]^T$, m is the mass of the shaft;
- $F_{unb} = [me\Omega^2\cos(\omega t) \quad me\Omega^2\sin(\omega t) \quad me\Omega^2\cos(\omega t) \quad me\Omega^2\sin(\omega t)]^T$, e is the residue distance, ω is the natural frequency of the unbalance force;
- $F_{mag} = [k_x x_d + k_i i_{dx} \quad k_x y_d + k_i i_{dy} \quad k_x x_{nd} + k_i i_{nx} \quad k_x y_{nd} + k_i i_{ny}]^T$, k_x is the stiffness gain and k_i is the current gain;
- F_w are the disturbance force on each axis.

In order to analyze the input-output relation with all internal states, the entire rotor AMB model can be described in the following matrix form,

$$\begin{bmatrix} \dot{x}_r \\ \dot{x}_s \\ \dot{x}_a \\ \dot{z}_1 \\ \dot{z}_2 \\ y \end{bmatrix} = \begin{bmatrix} A_r + B_{ri}k_xC_{sh} & 0 & B_{ri}k_iC_a & B_{rw} & 0 \\ B_sC_r & A_s & 0 & 0 & 0 \\ 0 & 0 & A_a & 0 & B_a \\ 0 & 0 & C_a & 0 & 0 \\ C_r & 0 & 0 & 0 & 0 \\ 0 & C_s & 0 & 0 & 0 \end{bmatrix} \begin{bmatrix} x_r \\ x_s \\ x_a \\ w \\ u \end{bmatrix},$$

where,

- u: control inputs,
- w: disturbance inputs,
- x_r: state vector of rotor node displacement,
- x_s: state vector of sensor measurement,
- x_a: state vector of amplifier voltage,
- z_1: amplifier current outputs,
- z_2: rotor displacement outputs,
- y: sensor measurement of shaft displacement;
- A_r, B_{ri}, B_{rw}, C_r come from the state space model of the rotor:

$$\dot{x}_r = A_r x_r + B_{ri} f + B_{rw} w,$$
$$z_2 = C_r x_r;$$

- A_a, B_a, C_a come from the state space model of the amplifier:

$$\dot{x}_a = A_a x_a + B_a u,$$
$$z_1 = C_a x_a;$$

- A_s, B_s, C_s come from the state space model of the sensor:

$$\dot{x}_s = A_s x_s + B_s C_r x_r,$$
$$y = C_s x_s;$$

- f is the control force generated by AMB:

$$f = k_x C_s h x_r + k_i C_a x_a.$$

A rotor AMB system diagram is shown in Fig. 4.4 and it can be observed that in order to find the input-output relation of such a system, we need not only the modeling of the AMB, but also many other components, which causes the entire model to be very complex and inconvenient for the controller design. Compared with the original model, the characteristic model can be easily applied

since the control objective is to attenuate the vibrations and keep shaft near the geometric center. It is essentially a position control scenario. Because AMBs are open-loop unstable, a feedback controller is required to keep them closed-loop stable. Based on the prerequisite presented earlier, a second order time-varying difference equation can be adopted to fulfill the modeling requirement for each axis and the four axes (DEX, DEY, NDEX, NDEY) are modeled using the characteristic modeling method. We will select the initial values of the characteristic parameters so that they can keep the second order system closed-loop stable. While $f_1(k_0)$ is close to 2 and $f_2(k_0)$ is negative but bigger than -1, both $g_0(k_0)$ and $g_1(k_0)$ should be much smaller than 1 according to the all-coefficient adaptive control method.

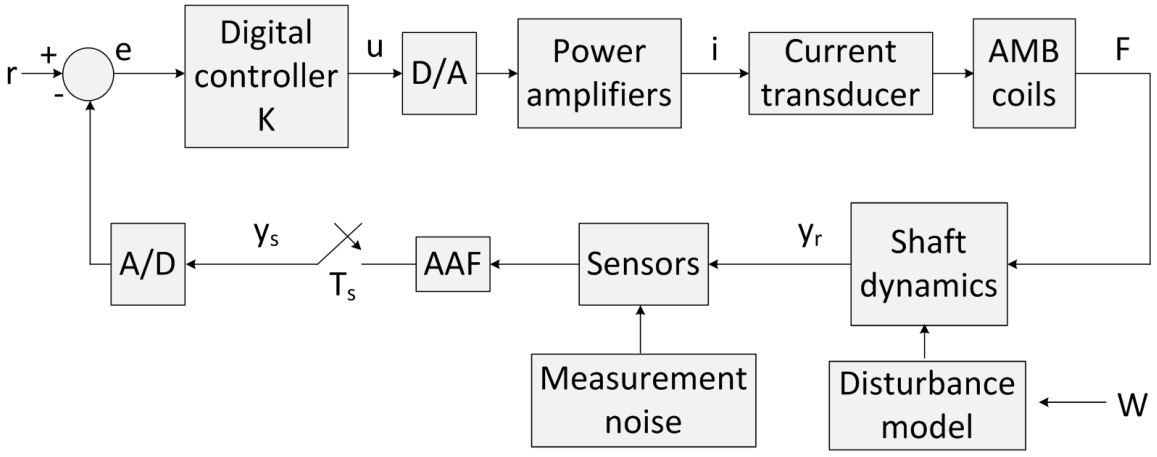

Figure 4.4: Rotor-AMB model diagram.

Based on the the characteristic modeling procedure shown in Chapter 3, a characteristic model for the rotor-AMB system is given as follows,

$$y(k) = f_1(k)y(k-1) + f_2(k)y(k-2) + g_0(k)u(k-1) + g_1(k)u(k-2),$$

and it can be parameterized as

$$y(k) = \theta^T(k)\phi(k), \tag{4.3}$$

where $f_1(k)$, $f_2(k)$, $g_0(k)$, $g_1(k)$ are the characteristic parameters and

$$\theta(k) = [f_1(k) \quad f_2(k) \quad g_0(k) \quad g_1(k)]^T, \tag{4.4}$$

$$\phi(k) = [y(k-1) \quad y(k-2) \quad u(k-1) \quad u(k-2)]^T. \tag{4.5}$$

The least-squares parameter estimation algorithm is described as below

$$\begin{aligned} N(k) &= \frac{P(k-1)\phi(k-1)}{\lambda + \phi^T(k-1)P(k-1)\phi(k-1)}, \\ P(k) &= \frac{1}{\lambda}[I - N(k)\phi^T(k)]P(k-1), \\ \hat{\theta}(k) &= \hat{\theta}(k-1) + N(k)[y(k) - \phi^T(k-1)\hat{\theta}(k-1)], \end{aligned}$$

where $\hat{\theta}(k)$ are estimates of the parameter vector $\theta(k)$ and λ is the forgetting factor and the estimation error is defined as

$$\epsilon(k) = y(k) - \phi^T(k)\hat{\theta}(k).$$

As shown in Fig. 4.5, a simulation scenario with the operation speed increasing from 0 to 18000 RPM is used to compare the original rotor AMB model with its characteristic model. The initial values of the characteristic parameters are chosen as $f_1(0) = 1.982$, $f_2(0) = -0.984$, $g_0(0) = 0.001$, $g_1(0) = 0.001$ and $\lambda = 0.975$, $P(0)$ is a 4×4 diagonal matrix with the diagonal values of 10. A robust control μ-synthesis is used to stabilize the rotor. During the simulation process, the rotor needs to pass two rigid modes (3515 RPM and 5789 RPM) and one flexible mode (14631 RPM) to reach 18000 RPM. By using the least-squares parameter estimation algorithm, the output of its characteristic model for four control axes (DEX, DEY, NDEX, NDEY) are consistently close to their original output for the entire speed range. Only when the speed surpasses the bending critical speed, for the worst case (NDEY), the tracking error gets slightly increased to around 0.04 mils (1 mil $= 2.54 \times 10^{-5}$ m) and remains below that level until 18000 RPM.

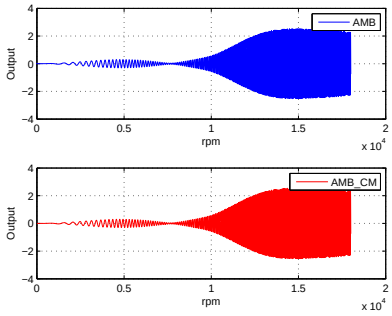

(a) System output (DEX).

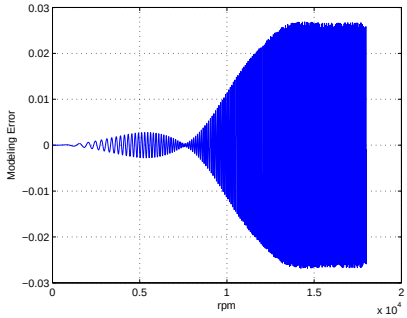

(b) Modeling error (DEX).

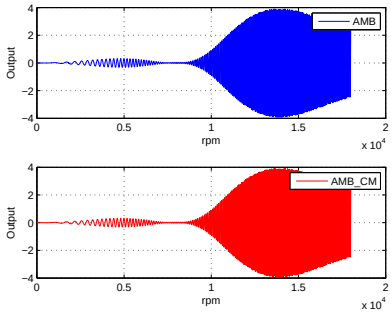

(c) System output (DEY).

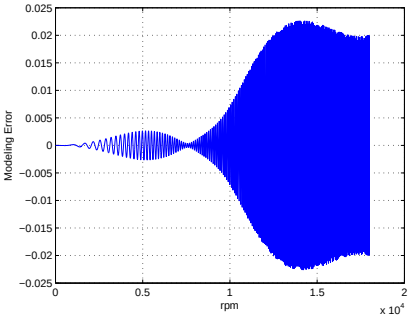

(d) Modeling error (DEY).

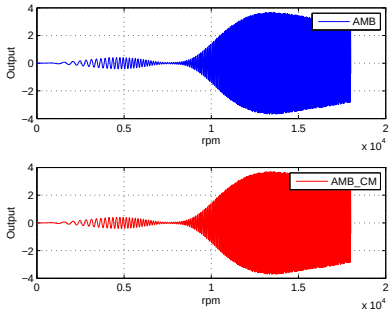

(e) System output (NDEX).

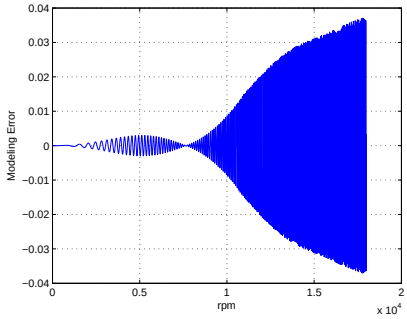

(f) Modeling error (NDEX).

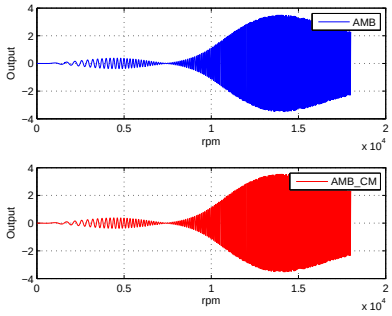

(g) System output (NDEY).

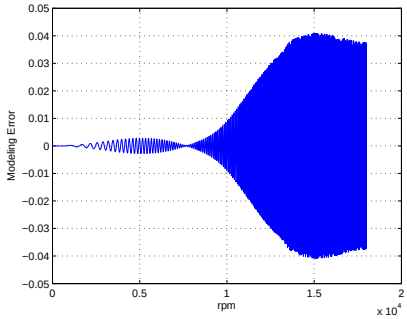

(h) Modeling error (NDEY).

Figure 4.5: Output comparisons between rotor-AMB model and the characteristic model.

4.4 Simulation and Experimental Results

In order to verify the proposed characteristic model based ACAC design, both simulation and experimental studies have been conducted. The simulation is based on the Simulink model derived for the entire rotor AMB system from [36], which includes all essential components of the test rig as shown in Fig. 4.6.

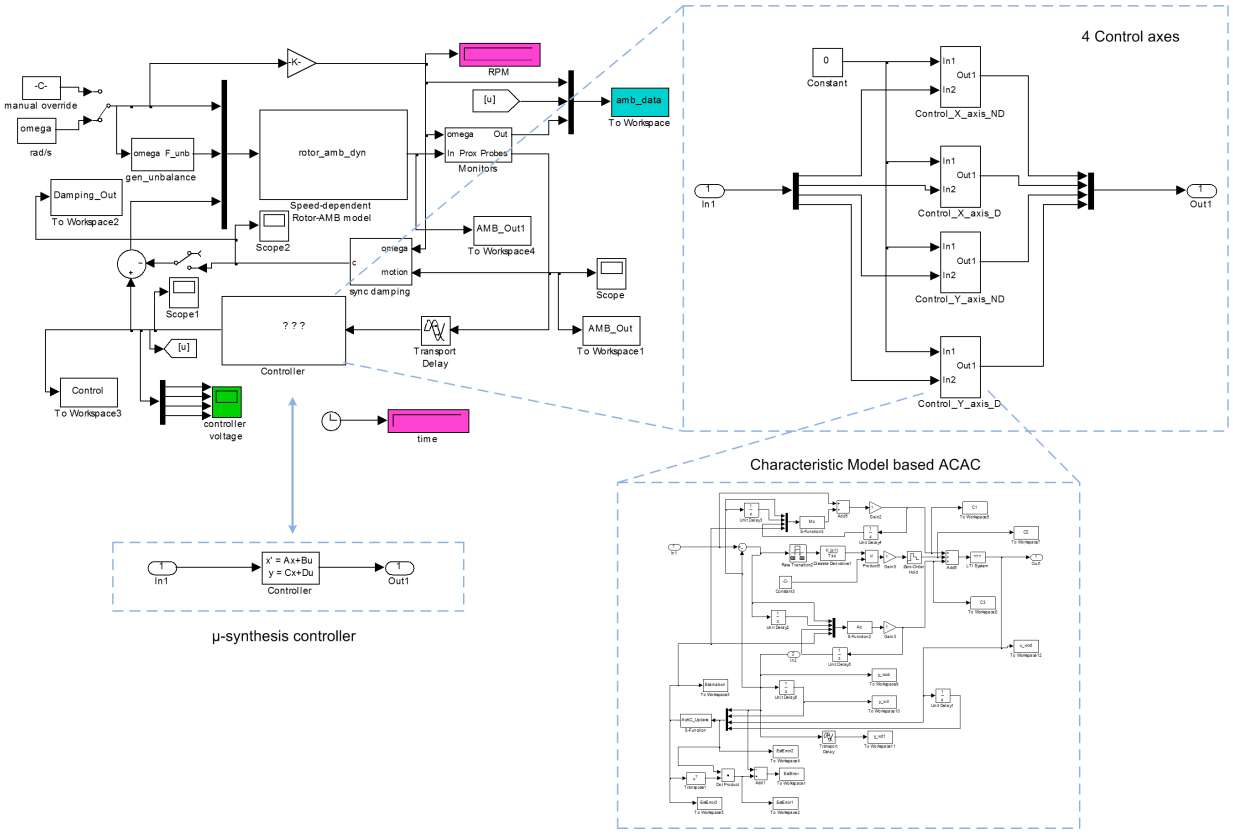

Figure 4.6: Simulation with simulink blocks.

The μ-synthesis controller was initially used to stabilize the test rig and its performance serves as a baseline for comparisons with our characteristic model based all-coefficient adaptive controller. In Simulink, the μ-synthesis controller is represented in a state space form with 48 states and 4 inputs and outputs. To verify the characteristic model based ACAC approach, the original μ-synthesis controller is replaced by the ACAC mechanism in Fig. 4.6. For the x and y axes of both driven and nondriven ends, characteristic model based ACAC with the same structure and controller parameters are utilized. The s-function in Simulink is used to implement the control and parameter estimation algorithms while the discrete-time controller has a sampling rate of 12 KHz. The sensor

measurements and control signals for all channels are saved into the workspace and the parameter estimates for entire characteristic parameters are also saved. In this simulation, we could adjust the rotating speed from 0 RPM to 18000 RPM or select a certain speed range and inspect the control performance in that speed range. In reality, the unbalance weight on our test rig disks could not be calibrated very accurately, so the simulated unbalance weight can also be adjusted to accommodate that limitation.

In the simulation, the initial values for the characteristic parameters are selected from the set N, where $1.9844 < f_1(k) < 2.2663$, $-1.2840 < f_2(k) < -1$, so $f_1(0) = 2.102$, $f_2(0) = -1.104$ and $g_0(0) = g_1(0) = 0.001$. Note that according to the all-coefficient adaptive control method,

$$f_1(0) + f_2(0) + g_0(0) + g_1(0) = 1.$$

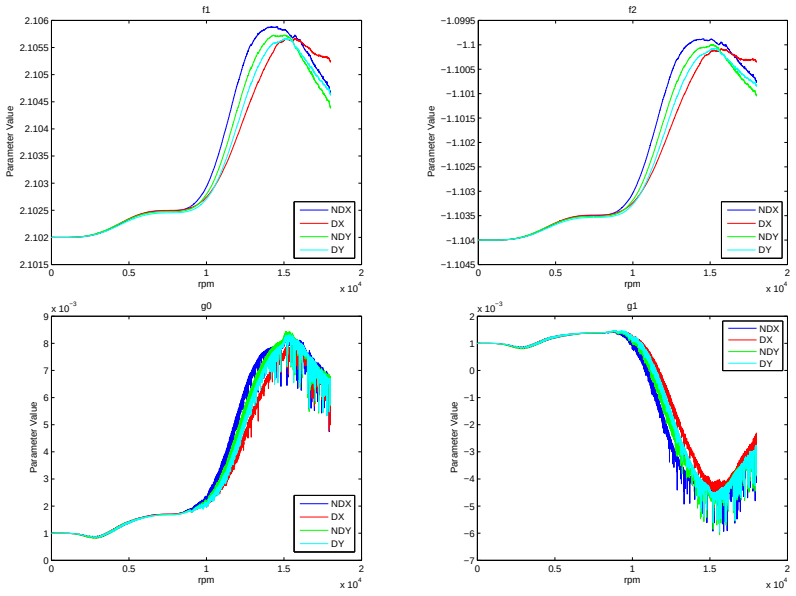

Figure 4.7: Parameter estimations from 0 RPM to 18000 RPM.

The controller parameters are chosen as $\lambda_1 = 0.16$, $d_1 = 0.0257$, $d_2 = 0.01$, $\delta = 3.5$ and $\gamma = 1.5$. The test starts with the rotating speed at 0 RPM and goes up to 18000 RPM, which passes the first bending critical speed at around 14800 RPM. The parameter estimations for the entire speed range are shown in Fig. 4.7, where with the change of the rotating speed, the controller parameters also get updated accordingly and remain bounded to guarantee a stable control performance. The parameter estimations for two operating speed cases at 9000 RPM and 14400 RPM are also shown

in Figs. 4.8 and 4.9, respectively. It is observed that the parameter estimation results are different for different operating speed cases. At 14400 RPM, the parameters converges within 0.5 seconds and remain bounded, while for the speed case at 9000 RPM, it takes longer for the parameter estimates to converge due to different system dynamics. It can be noticed that for different control channels, the control signals of ACAC remain bounded and they are very similar due to the same coefficient settings, while for the μ-synthesis, the control signals vary for different channels. In terms of the vibrations at both driven and nondriven ends, it can be observed that the displacements of x and y axes under control of ACAC remain bounded and they are much smaller than those using μ-synthesis for most of the speed range, which demonstrates the advantages using the characteristic model based ACAC controller. The simulation results are illustrated in Figs. 4.10 and 4.11.

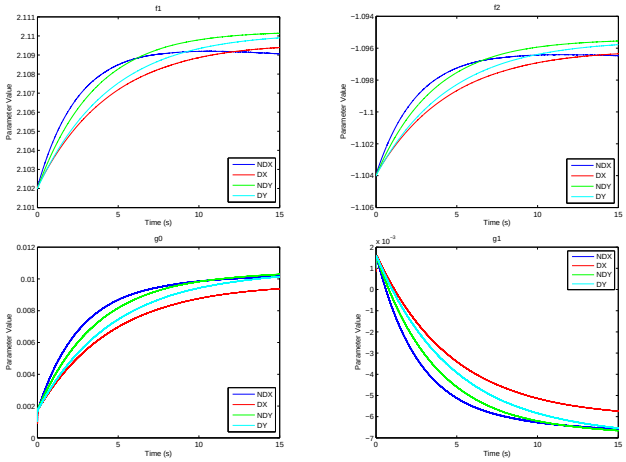

Figure 4.8: Parameter estimations at the operating speed of 9000 RPM.

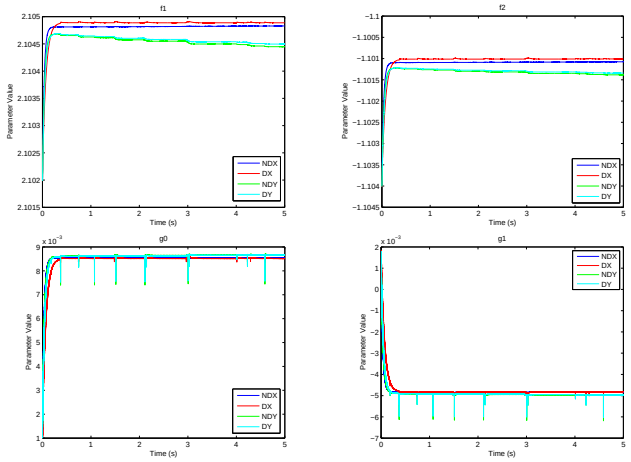

Figure 4.9: Parameter estimations at the operating speed of 14400 RPM.

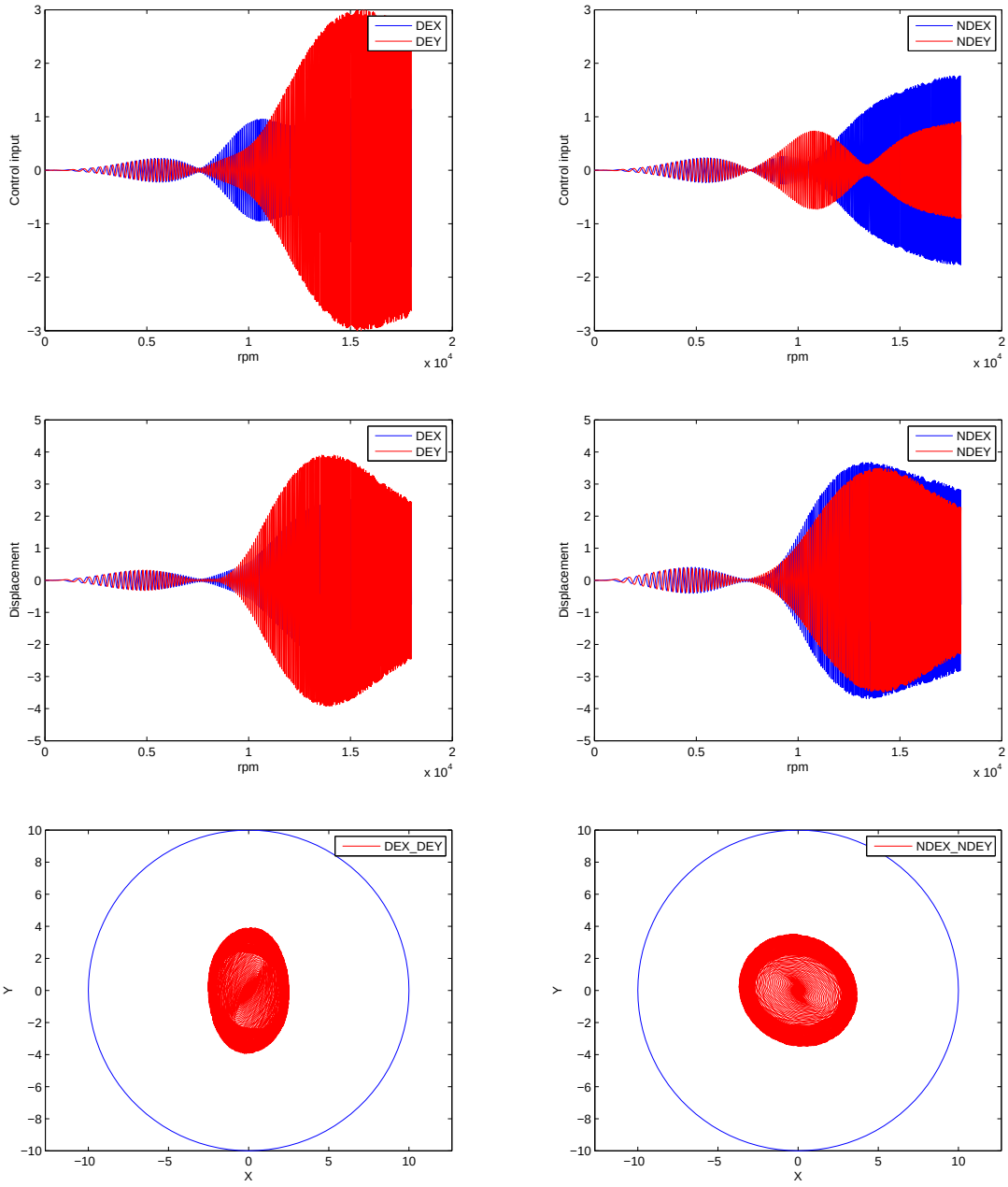

Figure 4.10: μ-synthesis simulation results (control inputs, shaft displacements and orbit size).

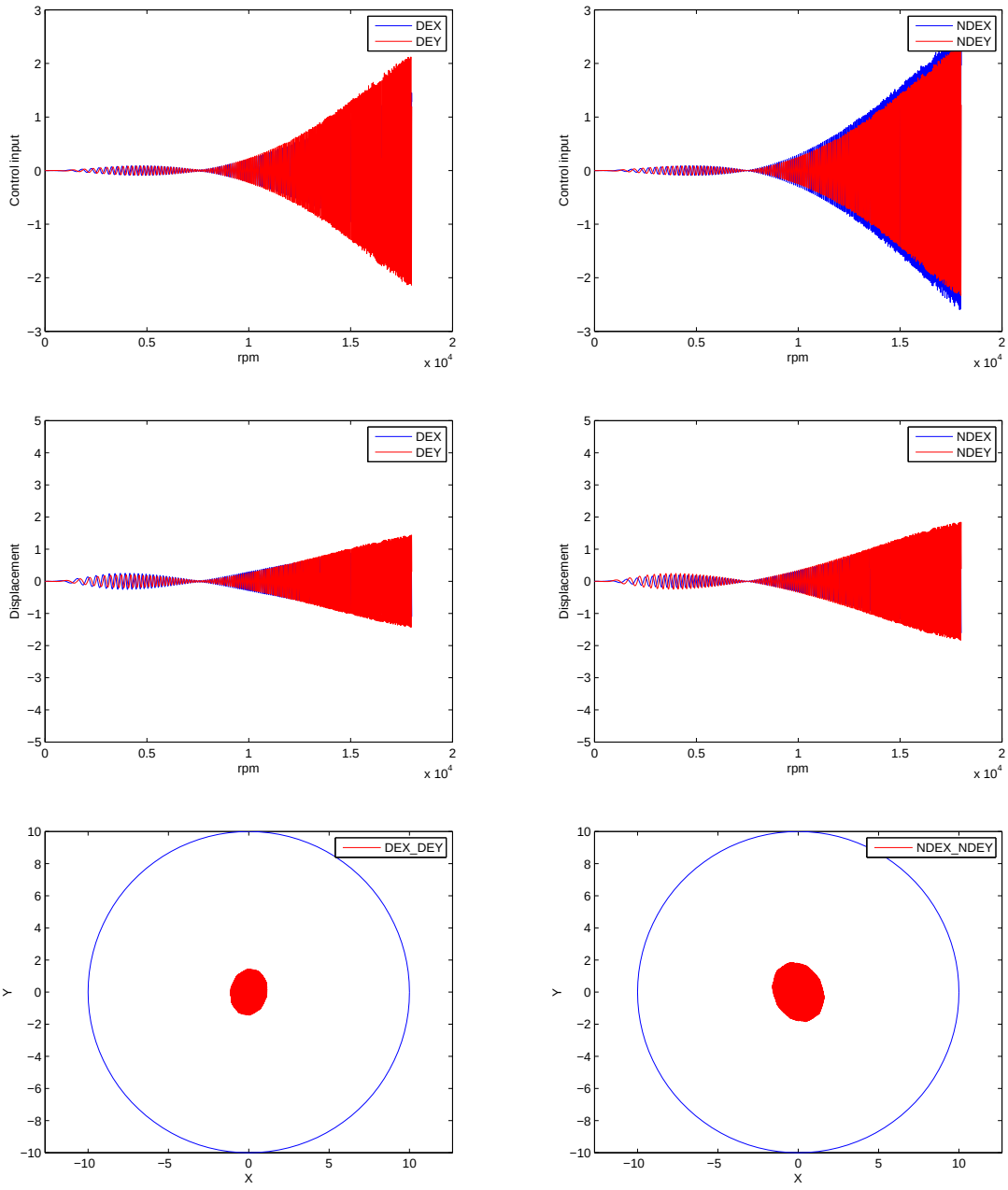

Figure 4.11: ACAC simulation results (control inputs, shaft displacements and orbit size).

After satisfactory simulation results were acquired, the characteristic model based ACAC algorithm was implemented on a DSP computer for the actual AMB test rig to verify the simulation results. Besides the DSP, a Labview data acquisition console is also added to interface with the computer for additional data logging. The data logging function is written in Labview 2010 and its block diagram is shown in Fig. 4.12. In this block diagram, the sensor measurements and

control outputs of all four control axes are saved at 6.4 KHz, which are much higher than the logging function provided by the DSP graphic user interface. They are also converted from the time domain response to the frequency domain response using the FFT block provided by Labview so it is possible to precisely identify at which frequency the maximum vibration happens. The rotating speed information is also logged at 6.4 KHz, so these information can be used to identify the unbalance weight and estimate the rotor stiffness and damping.

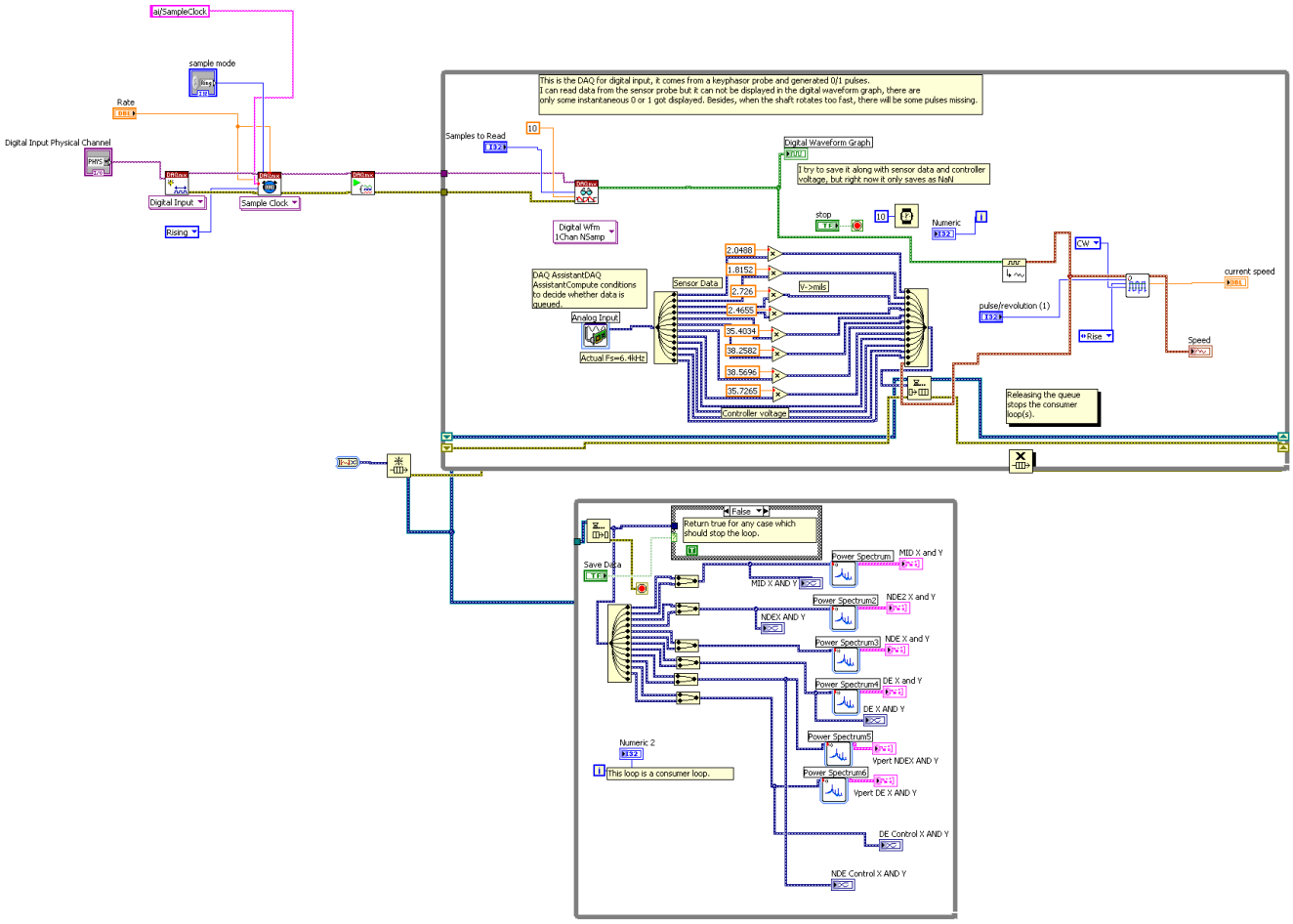

Figure 4.12: Labview block digram.

The same initial conditions and controller parameters used in the simulation are applied to the experiment. For practical implementation purposes, a first order low-pass filter combined with a phase bump filter is designed for rolling off the high frequency gains and performance compensation [37]. A notch filter is also added to attenuate the noise effect caused by the second bending mode

[38], which is around 530 Hz. The original ACAC algorithm is converted to C++ code and replaces the existing μ-synthesis algorithm. The recorded highest rotating speed is around 14400 RPM at which the rotor remains stable. 14400 RPM is quite close to the first bending mode of our test rig at 14800 RPM. ACAC approach preserves reliable performance and is comparable to the μ-synthesis in certain measures, as shown in Figs. 4.13 and 4.14.

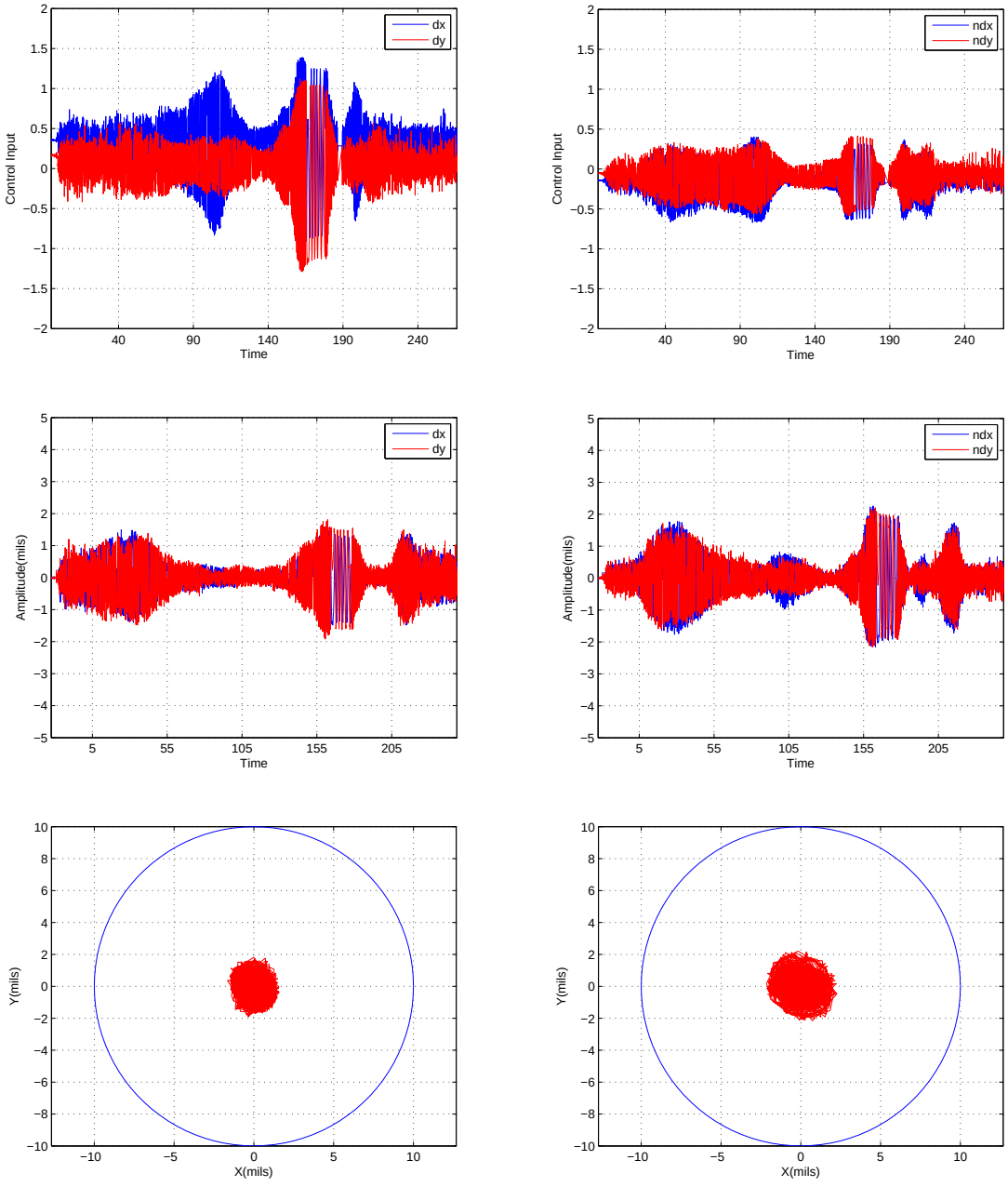

Figure 4.13: μ-synthesis experimental results (control inputs, shaft displacements and orbit size).

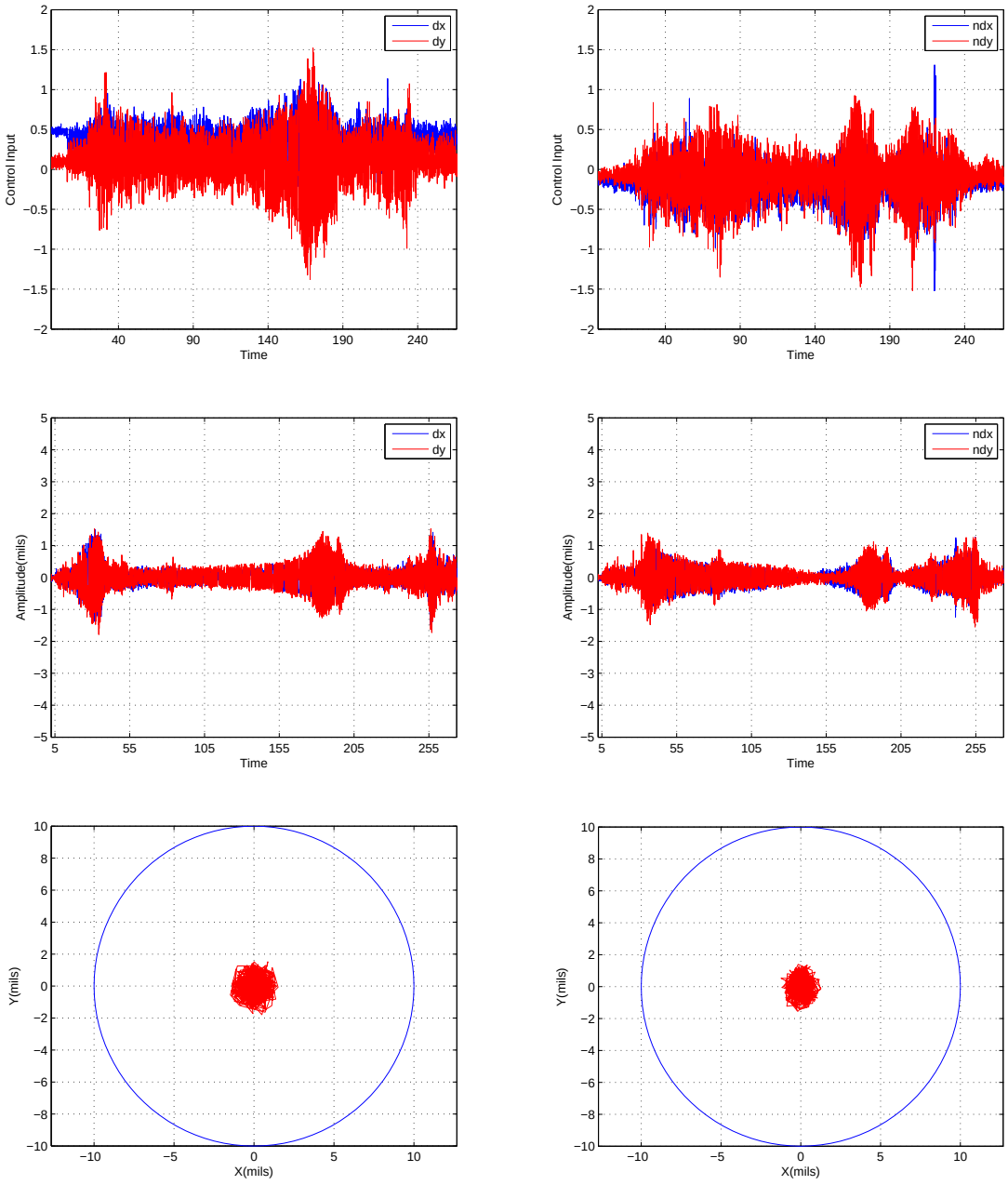

Figure 4.14: ACAC experimental results (control inputs, shaft displacements and orbit size).

It can be observed that for both ACAC method and μ-synthesis, the control signals have several peaks when the rotor passes through the rigid body modes at around 42 Hz and 83 Hz, the foundation mode at around 150 Hz, and moves towards the first bending mode. The control voltage of the μ-synthesis is smaller than the ACAC method and it also has a narrower bandwidth, which causes the operation to be quieter. In terms of vibration attenuation, the ACAC method is more effective

in both driven and nondriven ends by generating smaller rotating circles within 1.8 mils. When the operating speed reaches the first bending mode, the vibration level gets significantly increased, and the adaptation algorithm in the characteristic model based ACAC method cannot update the parameters fast enough and the controller is insufficient to effectively keep up with the vibration level increase. To address and overcome this limitation will be our future focus. Figs. 4.15 show the screenshots of the DSP graphic user interface for μ-synthesis and characteristic model based ACAC at the speed of 14400 RPM. It is shown that the orbit sizes for both driven end and nondriven end under the control of ACAC is much smaller than those under the control of μ-synthesis. In terms of controller outputs, the characteristic model based ACAC uses similar control voltage as the μ-synthesis for the driven end while for the nondriven end, the μ-synthesis uses smaller control voltage. The experimental results thus verify the performance of the characteristic model based ACAC. Therefore, this new control method has shown its strong potential for future research.

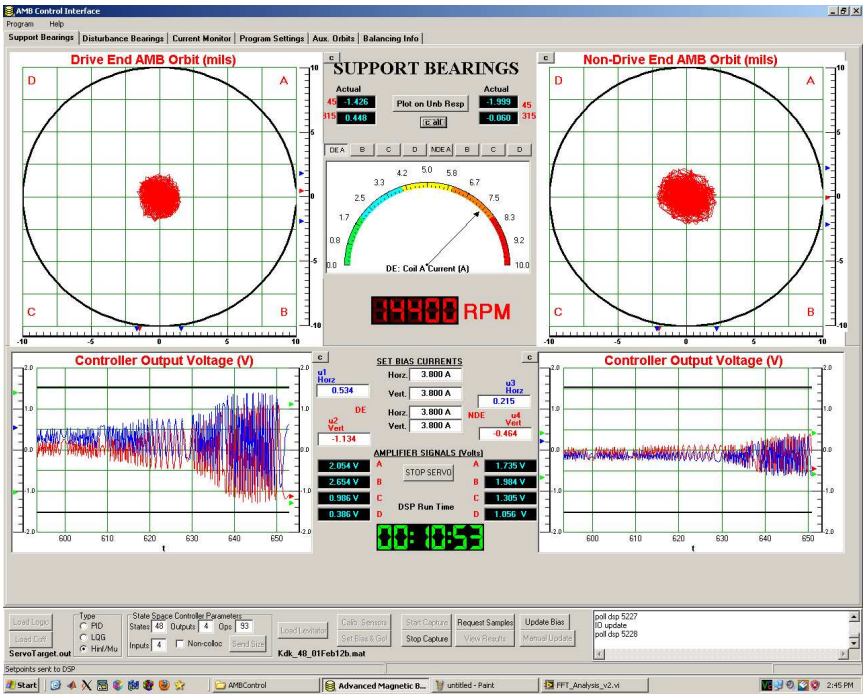

(a) μ-synthesis performance.

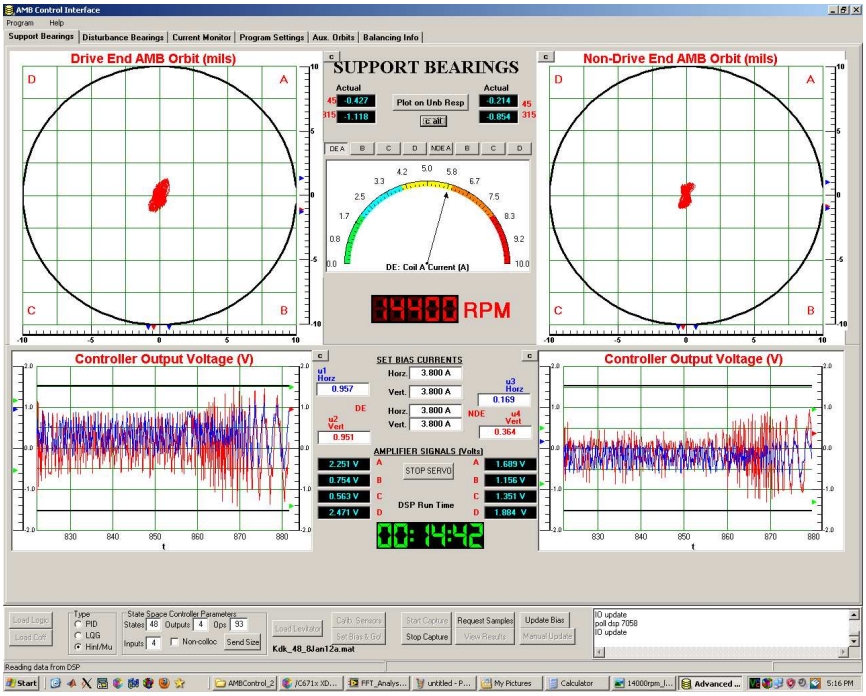

(b) Characteristic model based ACAC performance.

Figure 4.15: Experimental results at 14400 RPM.

Chapter 5

Conclusions

This thesis has presented the application of the characteristic model based all-coefficient adaptive control on a flexible rotor AMB system. Flexible rotor AMB system raises many challenges for control system designs. PID controller is simple and easy to implement but it is difficult to deliver robust control performance. Robust control μ-synthesis is able to better handle the uncertainties and to achieve reliable performance but it requires the plant and uncertainty models and the designed controller usually has high order. In order to find a suitable solution for flexible rotor AMB controls, the characteristic model based ACAC method is introduced. This method is able to provide robust control performance on systems with complex dynamics while maintaining a simple structure and not requiring the actual plant model.

In this thesis, the characteristic model based ACAC is used to stabilize a flexible rotor AMB test rig with the operating speed increasing from 0 RPM to 14400 RPM in the experiment. The all-coefficient adaptive control can guarantee not only the closed-loop stability but also sufficient performance during the transient process. The proposed characteristic modeling process significantly simplifies the modeling of a system with high order complex dynamics by analyzing its characteristics and considering the control requirement. A second order time-varying difference equation is able to model the rotor AMB system in a position tracking/keeping scenario. The characteristic model based ACAC method has been compared with an existing μ-synthesis controller in both simulations and experiments. The results verify the effectiveness of this new control method and show it is comparable to the μ-synthesis in certain measures. Therefore, the characteristic model based ACAC method has demonstrated its strong potential for future research.

Theoretical studies of the all-coefficient adaptive control and characteristic modeling methods will be the most important part in the future work. Addressing and resolving the performance limitation at the bending critical speed and applying this method to other AMB related platforms will be the focus for future work.

Bibliography

[1] Active magnetic bearing. http://www.engineerlive.com/Magnetic_Bearing_1_.jpg.

[2] Compressor applications. http://www.lonestarcompressor.com/new-compressor.jpg.

[3] Gas turbine. http://www.ge-energy.com/content/Gas-Turbine-Gen.jpg.

[4] G. Schweitzer and E. H. Maslen. *Magnetic Bearings*. Springer, 2009.

[5] E. H. Maslen and J. T. Sawicki. Mu-synthesis for magnetic bearings: Why use such a complicated tool? In *Proc. of the ASME 2007 Int. Mech. Eng. 843 Cong. and Expo. (IMECE07)*, page 11031112, Seattle, Washington, 2007.

[6] S. E. Mushi, Z. Lin, and P. E. Allaire. Design, construction, and modeling of a flexible rotor active magnetic bearing test rig. *IEEE/ASME Trans. Mechatronics*, PP(99):1–13, 2011.

[7] Guoxin Li. *Robust stabilization of rotor-active magnetic bearing systems*. PhD thesis, Univ. of Virginia, Charlottesville, VA, 2007.

[8] H. Wu, J. Hu, and Y. Xie. Characteristic model-based all-coefficient adaptive control method and its applications. *IEEE Trans. Systems, Man, and Cybernetics, Part C: Applications and Reviews*, 37(2):213–221, 2007.

[9] H. Wu, Y. Liu, Z. Liu, and Y. Xie. Characteristic modeling and the control of flexible structure. *Science in China Series: Information Sciences*, 44(4):278–291, 2001.

[10] G. Zhang, J. Liu, and H. Wu. Adaptive control of large flexible structures using the characteristic modeling technique. In *Proc. of IMACS Multiconference on "Computational Engineering in Systems Applications"(CESA)*, Beijing, China, Oct. 4-6, 2006.

[11] Z. Li, Z. Wang, and J. Li. A hybrid control scheme of adaptive and variable structure for flexible spacecraft. *Aerospace Science and Technology*, 8:423–430, 2004.

[12] Magnetic bearing. http://en.wikipedia.org/wiki/Magnetic_bearing.

[13] Benjamin C. Kuo. *Digital Control Systems*. Oxford University Press, 1992.

[14] T. Higuchi, T.Mizuno, and M. Tsukamoto. Digital Control System for Magnetic Bearings with Automatic Balancing. In *Proc. of the Second International Symposium on Magnetic Bearing*, University of Tokyo, Japan, July, 1990.

[15] C. R. Knospe, R. W. Hope, S. J. Fedigan, and R. D. Williams. Adaptive Online Rotor Balancing using Digital Control. In *Proc. of the "MAG '93" Conference and Exhibition for Magnetic Bearings, Magnetic Drives and Dry Gas Seals*, University of Virginia, USA, July, 1993.

[16] T. Higuchi, M. Otsuka, and T. Mizuno. Identification of Rotor Unbalance and Reduction of Housing Vibration by Periodic Learning Control in Magnetic Bearings. In *Proc. of the Third International Symposium on Magnetic Bearing*, University of Virginia, USA, July, 1992.

[17] Y. Kanemitsu, M. Ohsawa, and K. Watanabe. Real Time Balancing of a Flexible Rotor supported by Magnetic bearings. In *Proc. of the Second International Symposium on Magnetic Bearing*, University of Tokyo, Japan, July, 1990.

[18] H. Habermann and M. Brunet. The Active Magnetic Bearing Enables Optimum Damping of Flexible Rotors. In *Proc. of the ASME International Gas Turbine Conference*, Amsterdam, Netherlands, 1994.

[19] C. R. Burrows, N. Sahinkaya, A. Traxler, and G. Schweitzer. Design and Application of a Magnetic Bearing for Vibration Control and Stabilization of a Flexible Rotor. In *Proc. of the First International Symposium on Magnetic Bearings*, ETH *Zürich*, Switzerland, June 1988.

[20] K. Nonami and T. Ito. μ Synthesis of Flexible Rotor-Magnetic Bearing Systems. *IEEE Trans. Contr. Syst. Technol*, 3:202–211, 1996.

[21] H. Shida, M. Ichihara, and K. Seto. Motion and Vibration Control of Flexible Rotor Using Magnetic Bearings. In *Proc. of the 8th International Symposium on Magnetic Bearing*, Mito, Japan, August 26-28, 2002.

[22] H. Fujiwara, K. Ebina, M. Ito, N. Takahashi, and O. Matsushita. Control of Flexible Rotors Supported by Magnetic Bearings. In *Proc. of the 8th International Symposium on Magnetic Bearing*, Mito, Japan, August 26-28, 2002.

[23] S. Lei and A. Palazzolo. Control of Flexible Rotor System with Active Magnetic Bearings. *Journal of Sound and Vibration*, 314(1-2):19–38, 2008.

[24] H. Wu and Z. Sha. An all-coefficient adaptive control method. *ACTA AUTOMATICA SINICA*, 11(1):12–20, 1985.

[25] C. Qi, H. Wu, and Z. Lv. The study on the stability of all-coeficient golden section feedback control system. In *Proc. of the 3rd World Congress on Intelligent Control and Automation*, Hefei, China, June 28-July 2, 2000.

[26] Hu Jun. All Coefficients Adaptive Reentry Lifting Control of Manned Spacecraft. *Journal of Astronautics*, 191, 1998.

[27] Hongxin Wu, Jun Hu, and Yongchun Xie. *Characteristic Model-Based Intelligent Adaptive Control*. China Science and Technology Press, 2008.

[28] Xie Yongchun and Wu Hongxin. The Robustness of the All-coefficient Adaptive Control Method. *SCIENCE CHINA: Information Sciences*, 23(2), 1997.

[29] Xie Yongchun and Wu Hongxin. The Application of the Golden Section in Adaptive Robust Controller Design. *ACTA AUTOMATICA SINICA*, 18, 1992.

[30] Gang Tao. *Adaptive Control Design and Analysis*. Wiley, 2003.

[31] B. Meng, H. Wu, Z. Lin, and G. Li. Characteristic model based control of the x-34 reusable launch vehicle in its climbing phase. *Science in China Series F: Information Sciences*, 52(11):2216–2225, 2009.

[32] Bin Meng and Hong-Xin Wu. A Unified Proof of the Characteristic Model of Linear Time-Invariant Systems. In *Proc. of the 2007 American Control Conference*, pages 935–940, New York City, USA, July 11-13, 2007.

[33] Shen Shaoping and Wu Hongxin. The Application of Adaptive Control Method Based on Characteristic Model in Vibration Suppression of the Cantilever Beam. In *Proc. of 25th Chinese Control Conference*, Harbin, Heilongjiang, August, 2006.

[34] Zhang Zhao and Hu Jun. Stability Analysis of a Hypersonic Vehicle Controlled by the Characteristic Model based Adaptive Controller. *SCIENCE CHINA: Information Sciences*, 55(10):22432256, 2012.

[35] S. E. Mushi. Control of flexible rotors supported by active magnetic bearings. Master's thesis, Univ. of Virginia, Charlottesville, VA, 2008.

[36] S. E. Mushi. *Robust control of rotordynamic instability in rotating machinery supported by active magnetic bearings*. PhD thesis, Univ. of Virginia, Charlottesville, VA, 2012.

[37] H. Fujiwara, K. Ebina, K. Ebina, and O. Matsushita. Control of flexible rotors supported by active magnetic bearings. In *Proc. of 8th Int. Symposium on Magnetic Bearings*, pages 145–150, Mito, Japan, August 26-28, 2002.

[38] S. E. Mushi, Z. Lin, and P. E. Allaire. Design, construction and modeling of a flexible rotor active magnetic bearing test rig. In *Proc. of ASME Turbo Expo 2010: Power for Land, Sea and Air*, Glasgow, UK, June 14-18, 2010.

[39] G.K. Egan and B. Taylor. The Use of Infrared Sensors for Absolute Attitude Determination of Unmanned Aerial Vehicles. Tech. Rep. MECSE-22-2006, Monash University, Australia, 2006.

[40] Z. Li, Z. Wang, and J. Li. Modeling of a high speed rotor test rig with active magnetic bearings. *ASME J. of Vibration and Acoustics*, 128(3):269–281, 2006.

[41] Y. Lei and H. Wu. Tracking control of robotic manipulators based on the all-coefficient adaptive control method. *International Journal of Control, Automation, and Systems*, 4(2):139–145, 2006.

[42] Wu Hongxin, Xie Yongchun, Li Zhibin, and He Yingzi. Intelligent Control Based on Description of Plant Characteristic Model. *ACTA AUTOMATICA SINICA*, 25, 1999.

[43] Gene F. Franklin, J. David Powell, and Abbas Emami-Naeini. *Feedback Control of Dynamic Systems*. Prentice Hall, 2009.

[44] Chi-Tsong Chen. *Linear System Theory and Design*. Oxford, 1999.